ESC European Society of Cardiology

Cardiovascular Research (2024) **00**, 1–20
https://doi.org/10.1093/cvr/cvae102

miR-369-3p ameliorates diabetes-associated atherosclerosis by regulating macrophage succinate-GPR91 signalling

Shruti Rawal[1], Vinay Randhawa[1], Syed Husain Mustafa Rizvi[2,3], Madhur Sachan[1], Akm Khyrul Wara[1], Daniel Pérez-Cremades[1,4], Robert M. Weisbrod[2,3], Naomi M. Hamburg[2,3], and Mark W. Feinberg [1]*

[1]Cardiovascular Division, Department of Medicine, Brigham and Women's Hospital, Harvard Medical School, 77 Avenue Louis Pasteur, Boston, MA 02115, USA; [2]Vascular Biology Section, Boston University School of Medicine, Boston, MA, USA; [3]Cardiology, Whitaker Cardiovascular Institute, Boston University School of Medicine, Boston, MA, USA; and [4]Department of Physiology, University of Valencia, INCLIVA Biomedical Research Institute, Valencia 46010, Spain

Time of primary review: 17 days

Online publish-ahead-of-print 4 May 2024

Aims

Diabetes leads to dysregulated macrophage immunometabolism, contributing to accelerated atherosclerosis progression. Identifying critical factors to restore metabolic alterations and promote resolution of inflammation remains an unmet goal. MicroRNAs orchestrate multiple signalling events in macrophages, yet their therapeutic potential in diabetes-associated atherosclerosis remains unclear.

Methods and results

miRNA profiling revealed significantly lower miR-369-3p expression in aortic intimal lesions from *Ldlr–/–* mice on a high-fat sucrose-containing (HFSC) diet for 12 weeks. miR-369-3p was also reduced in peripheral blood mononuclear cells from diabetic patients with coronary artery disease (CAD). Cell-type expression profiling showed miR-369-3p enrichment in aortic macrophages. *In vitro*, oxLDL treatment reduced miR-369-3p expression in mouse bone marrow-derived macrophages (BMDMs). Metabolic profiling in BMDMs revealed that miR-369-3p overexpression blocked the oxidized low density lipoprotein (oxLDL)-mediated increase in the cellular metabolite succinate and reduced mitochondrial respiration (OXPHOS) and inflammation [Interleukin (IL)-1β, TNF-α, and IL-6]. Mechanistically, miR-369-3p targeted the succinate receptor (GPR91) and alleviated the oxLDL-induced activation of inflammasome signalling pathways. Therapeutic administration of miR-369-3p mimics in HFSC-fed Ldlr–/– mice reduced GPR91 expression in lesional macrophages and diabetes-accelerated atherosclerosis, evident by a decrease in plaque size and pro-inflammatory Ly6C^{hi} monocytes. RNA-Seq analyses showed more pro-resolving pathways in plaque macrophages from miR-369-3p-treated mice, consistent with an increase in macrophage efferocytosis in lesions. Finally, a GPR91 antagonist attenuated oxLDL-induced inflammation in primary monocytes from human subjects with diabetes.

Conclusion

These findings establish a therapeutic role for miR-369-3p in halting diabetes-associated atherosclerosis by regulating GPR91 and macrophage succinate metabolism.

Downloaded from https://academic.oup.com/cardiovascres/advance-article/doi/10.1093/cvr/cvae102/7664626 by Ewha Womans University user on 02 September 2024

* Corresponding author. Tel: 617 525 4381; fax: 617 525 4380, E-mail: mfeinberg@bwh.harvard.edu

© The Author(s) 2024. Published by Oxford University Press on behalf of the European Society of Cardiology. All rights reserved. For commercial re-use, please contact reprints@oup.com for reprints and translation rights for reprints. All other permissions can be obtained through our RightsLink service via the Permissions link on the article page on our site—for further information please contact journals.permissions@oup.com.

Graphical Abstract

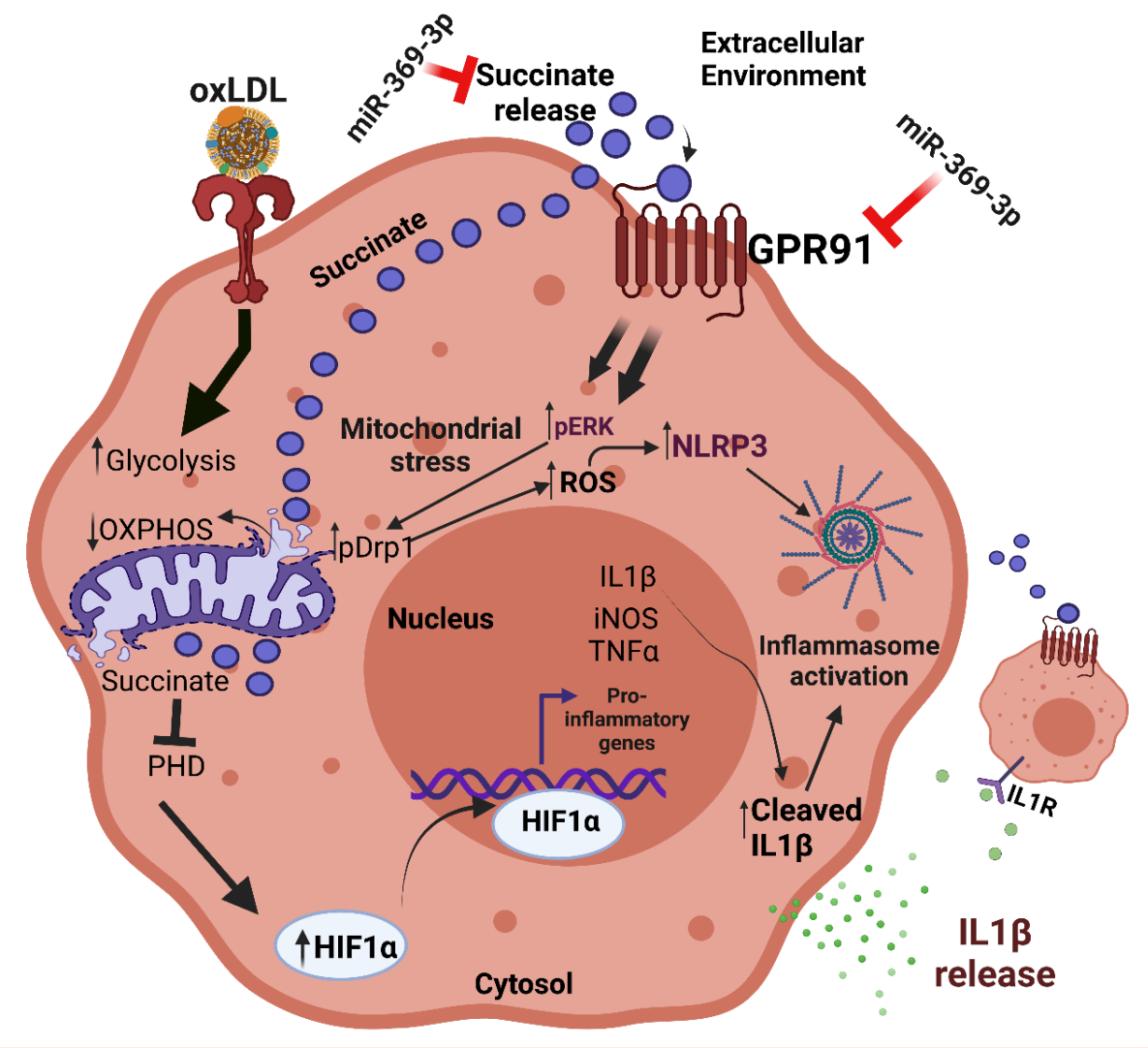

Keywords microRNA • Diabetes • Atherosclerosis • Macrophage • GPR91 • Succinate

1. Introduction

People with Type 2 diabetes suffer a higher burden from cardiovascular disease (CVD).[1,2] The presence of diabetes or insulin resistance has been associated with accelerated coronary events and adverse clinical outcomes when compared to age-matched non-diabetic individuals.[3] Statins have been shown to lower the relative risk of CVD in patients with diabetes, but the absolute risk remains higher compared to non-diabetics. These results imply that diabetes-associated atherosclerosis involves molecular processes that impair favourable effects of lipid and glucose normalization on plaque immune cells, especially macrophages that are major drivers of inflammation.

Hyperglycaemia–induced oxidative stress modifies LDL-C into an oxLDL form.[4] During the initial phase of development of atherosclerotic lesions, circulating monocytes adhere to the endothelium and enter into the vessel wall followed by differentiation into macrophages. These macrophages take up excess oxLDL through scavenger receptors and become lipid-laden foam cells. Furthermore, macrophage-rich lesions are associated with plaque rupture and induce the acute clinical complications of atherosclerosis: myocardial infarction and stroke.[5] Hyperglycaemia promotes epigenetic and metabolic reprogramming in macrophages that triggers persistent inflammation even after achieving normoglycemic levels.[6,7] Therefore, there is a critical need to develop tailored approaches that precisely target the molecular alterations underlying this immune-metabolic dysregulation. Recent reports indicate that pro-inflammatory immunometabolites fuel macrophage inflammation because of metabolic dysfunction.[8] Notably, under hyperglycaemic conditions, macrophages undergo genetic and epigenetic modifications, resulting in open chromatin regions that favour transcription of several inflammatory genes.[9,10] Identifying altered immunometabolites and their downstream pro-inflammatory signalling pathways provide opportunities for therapeutic targeting to help restore metabolic homeostasis.

It is well known that diabetic macrophages are more glycolytic, increasing reactive oxygen species (ROS) production, favouring a

Downloaded from https://academic.oup.com/cardiovascres/advance-article/doi/10.1093/cvr/cvae102/7664626 by Ewha Womans University user on 02 September 2024

pro-inflammatory phenotype. However, the mechanisms pertaining to this phenotype remain obscure. Reports suggest that disruption of the citric acid/trichloroacetic acid (TCA) cycle contributes to accumulation of several key pro-inflammatory metabolites, including but not limited to succinate, malonate, fumarate, in macrophages and dendritic cells.[11–13] These metabolites are known to act through specific receptors. For example, succinate binds to the G-coupled receptor GPR91 and promotes inflammation by stabilizing HIF-1α and inflammasome activation.[14] Identifying key regulators that could block this pathway and maintain or restore metabolic homeostasis remains an active area of investigation.

Non-coding RNAs, including microRNAs (miRNAs) and long non-coding RNAs act as rheostats of several biological pathways and provide new therapeutic targets and as potential diagnostic biomarkers for CVD.[15–23] miRNAs act as master regulators to control a large variety of biological processes including inflammation and the metabolic state of immune cells by regulating key inflammatory and metabolic genes, and their mis-expression in diabetes can be both informational and causal.[24–26] Because of their selectivity and specificity, miRNAs comprise potential useful therapeutic targets in the effort towards achieving precision medicine, especially given their central role in regulating key metabolic pathways.[27,28] Although recent studies have demonstrated the role of miRNAs in the progression of atherosclerosis in mice (e.g. miR-21[18] and miR-33,[19,29]) their role in diabetes-associated atherosclerosis remains poorly understood. The current work elucidated the role of one such miRNA, miR-369-3p, in regulating the key processes involved in the progression of diabetes-associated atherosclerosis. miRNA-seq profiling of intimal lesions of *Ldlr*−/− mice on a high-fat, high sucrose-containing (HFSC) diet revealed that miR-369-3p was markedly down-regulated with atherosclerotic progression. Similarly, miR-369-3p was significantly down-regulated in peripheral blood mononuclear cells (PBMCs) from patients with diabetes or diabetes-associated CVD. Furthermore, miR-369-3p was highly expressed in the myeloid compartment, particularly in macrophages. In this study, miR-369-3p was found to play a central role in regulating immunometabolic rewiring of macrophages and diabetes-associated atherosclerosis by regulating a succinate-GPR91- HIF-1α-inflammasome signalling axis.

2. Methods

2.1 Bone marrow-derived macrophage cultures

Bone marrow-derived macrophages (BMDMs) were isolated and differentiated as previously described.[30] Briefly, bone marrow cells were isolated by flushing from the femur and tibia of C57BL/6 mice. Cells were differentiated into BMDMs in 4.5 g/L glucose Dulbecco's modified Eagle's medium (DMEM) (#, Gibco) supplemented with 10 ng/mL mouse macrophage colony stimulation factor (#315-02, Peprotech), 10% Fetal Bovine Serum (FBS), and 1% Penicillin–Streptomycin antibiotic at 37°C and 5% CO_2 for 7 days.

2.2 Cell transfection and treatments

BMDMs were transfected with non-specific (NS) control mimic or mmu-miR-369-3p (369-m) mimic (miRvana) at a concentration of 30 nM or with NS control inhibitor or mmu-miR-369-3p inhibitor (mirVana) at a concentration of 100 nM using Lipofectamine RNAiMAX, as previously described.[31] Briefly, transfection of macrophages was performed in OPTIMEM media overnight. The next day, the same volume of DMEM containing 10% (*v*/*v*) FBS was added. After transfection for 48 h, cells were serum-starved overnight using DMEM medium with 0.2% Bovine serum albumin (BSA) and then exposed to oxLDL (Invitrogen, L34357) for 24 h and collected for further experiments. Similarly, macrophages were transfected with 10 nM negative (non-silencing) control siRNA or sucnr1 (GPR91) siRNA (Smartpool siRNA, Dharmacon) for 48 h and then exposed to oxLDL for 24 h. For some experiments, BMDMs were pretreated with 3 mM *N*-acetyl cysteine (NAC), an antioxidant or with 10 mM dimethyl malonate (DMM), a succinate dehydrogenase (SDH) inhibitor for 2 h prior to oxLDL-treatment. Briefly, after 2 h of NAC or DMM incubation, the media was replaced with fresh media (DMEM medium with 0.2% BSA) and cells were then treated with oxLDL for 24 h.

2.3 western blot analysis

Cells were washed in ice-cold phosphate buffered saline (PBS) and lysed in ice-cold radio-immunoprecipitation assay buffer supplemented with protease and phosphatase inhibitor cocktail (Cell Signalling). Protein concentrations were determined using Pierce BCA assay (Thermo Fisher Scientific, Waltham MA, USA). In total, 50 μg proteins were loaded per lane on a 4–20% Mini-PROTEAN TGX Gel (Bio-Rad, 456-1096). Separated proteins were transferred to polyvinylidene fluoride membranes using the Transfer Turbo Blot system (Bio-Rad) and Trans-Blot Turbo RTA Transfer Kit (Bio-Rad, 170-4272). The membrane was blocked with 5% non-fat milk in Tris-buffered saline with 0.1% Tween® 20 Detergent for 1 h at room temperature. After blocking, the membrane was incubated overnight at 4°C with antibodies against GPR91 (Novus Biologicals, 1:1 000), phosphor-p65 (Cell Signalling, 1:500), total p65 (Cell Signalling, 1:1 000), HIF-1α (Novus Biologicals, 1:5 000), phosphor-ERK1/2 (Cell Signalling, 1:1 000), total ERK1/2 (Cell Signalling, 1:1 000), phosphor-DRP1 (Cell Signalling, #, 1:500), total DRP1 (Cell Signalling, 1:1 000), HRP-conjugated β-actin (Cell Signalling, 1:10 000), cleaved Interleukin (IL)-1β (Cell Signalling, 1:500), or cleaved caspase 1 (Cell Signalling, 1:1 000).

2.4 Mitochondrial bioenergetics: seahorse assay

Mitochondrial oxygen consumption rates (OCR) and extracellular acidification rates (ECAR) were determined using an XF24-well Analyzer (Agilent, CA).[32] Differentiated BMDMs were seeded at 1×10^6 cells/well in XF24-well plates (Agilent) and transfected with non-specific control mimic (NS-m) or miR-369-3p mimic followed by oxLDL-loading, as described above. Wells without cells were included as a background control. Mitochondrial OCR was measured and plotted at basal conditions followed by sequential addition of 2 μg/mL oligomycin (ATP synthase inhibitor), 1 μmol/L FCCP (carbonylcyanide-p-trifluoromethoxyphenylhydrazone) (a mitochondrial uncoupler), and 0.5 μmol/L rotenone (complex I inhibitor) plus 0.5 μmol/L antimycin A (complex III inhibitor). Glycolytic capacity of BMDMs was determined by Seahorse XF Glycolysis Stress Test Kit (Agilent Technologies) according to the manufacturer's instructions. For the measurement of ECAR, XF base media (Agilent, CA #102353-100) was supplemented sequentially with 25 mM glucose and 2 mM L-glutamine, oligomycin (1 μM), and 2-DG (30 mM) (Sigma-Aldrich, St. Louis, MO) to measure glycolysis, glycolytic capacity, and glycolytic reserve, respectively. Total protein content was measured from each well using BCA assay and used to normalize the Seahorse data.

2.5 Metabolite analysis

Polar metabolites were quantitatively profiled by a positive/negative ion–switching, targeted liquid chromatography tandem mass spectrometry (LC–MS/MS) based metabolomics platform using a 5500 QTRAP hybrid triple quadruple mass spectrometer (AB/SCIEX) via selected reaction monitoring (SRM) as described previously.[33] Briefly, BMDMs were transfected with NS or miR-369-3p mimic for 48 h followed by exposing to oxLDL for 24 h, as described above. The supernatants were collected and subjected to methanol extraction using 80% (*v*/*v*) methanol (−80°C). The insoluble extracted material was immediately pelleted in a cooled centrifuge (4°C). The supernatants were lyophilized using a SpeedVac concentrator using no heat. LC/MS grade water (20 μL) were added to resuspend each sample just before LC–MS/MS analysis and 5 μL of sample were injected onto the autosampler of the LC system (Shimadzu) using an amide HILIC column (Waters). Once the SRM data for ~285 metabolites were acquired, peaks were integrated using a software platform for peak area integration MultiQuant 2.1 (AB/SCIEX). Paired *t*-test was implemented on the metabolite expression values to compute the fold-change and significance (*P*-values) in groups NS-oxLDL vs. NS-BSA and 369-m-oxLDL vs. NS-oxLDL. To display the number of group-specific and common metabolites between NS-oxLDL vs. NS-BSA and 369-m-oxLDL vs.

Downloaded from https://academic.oup.com/cardiovascres/advance-article/doi/10.1093/cvr/cvae102/7664626 by Ewha Womans University user on 02 September 2024

NS-oxLDL, Venn diagram was created. Further, respective barplot of 13 commonly altered metabolites between groups was also plotted. Lastly, the association between commonly altered metabolites and the metabolic pathways was derived using Kyoto Encyclopedia of Genes and Genomes (KEGG) (https://www.genome.jp/kegg/pathway.html) pathway analyses on the MetaboAnalyst (version 5.0) (https://academic.oup.com/nar/article/49/W1/W388/6279832) web-based platform. Enrichment of pathways was evaluated using hypergeometric test to compute the *P*-values based on the number of metabolites associated per pathway. The pathways along with metabolites were presented as a Chordplot, which was generated by R-Circlize (version 0.4.15) library (https://www.rdocumentation.org/packages/circlize).

2.6 Primary mouse monocytes isolation and succinate treatment

Primary mouse monocytes were isolated from bone marrows of 8-week-old male C57Bl6 mice, using MACs isolation kit for negative selection of monocytes (Cat# 130-100-629; Miltenyi Biotec GmbH, Bergisch Gladbach, Germany). The approximate yield of monocytes from one bone marrow of one mouse was 4×10^7 cells/mL. The purity of monocytes was first confirmed using flow cytometry analyses. Cells were stained with Fixable Viability Dye Zombie yellow orange (Biolegend, San Diego, CA) for 30 min on ice followed by staining with fluorescence-conjugated antibodies for surface markers: Phycoerythrin (PE) anti-mouse CD115 and Allophycocyanin (APC) anti-mouse Ly6C (monocyte-specific markers) and APC/Cy7 anti-mouse Ly6G (a neutrophil marker) from Biolegend, CA. Approximately 87% of live cells were CD115 + Ly6C + Ly6G−. Once the purity of isolations was established, fresh cells were seeded in 6-well plates (5×10^5 cells/well) and were stimulated with 200 μM succinate for 2 h prior to exposing them to oxLDL-treatment for 24 h. Cells were harvested and supernatants were collected for further experiments.

2.7 Bioinformatic analyses for identification of putative target genes for miR-369-3p

To determine the conserved putative target genes of miR-369-3p between mouse (*Mus musculus*) and human (*Homo sapiens*), the predicted interactions were retrieved from TargetScan (Release 7.1) database (cite: https://pubmed.ncbi.nlm.nih.gov/26267216/). The miRNA-gene pairs with low weighted context score (<−0.05) were removed during the analysis. The mouse and human prediction datasets were overlapped, and the common target genes were identified. Significantly enriched biological terms associated with the sorted genes were determined by performing Gene ontology (GO) enrichment analyses using R-GOstats (version 0.4.15) library (https://bioconductor.org/packages/release/bioc/html/GOstats.html). Significantly enriched (False Discovery Rate adjusted *P*-value <0.05) biological process (BP) terms were obtained against the mouse genome background. Among the list of enriched BP terms, we prioritized the list of targets that were associated with the GO term 'regulation of inflammatory response' (GO: 0050727). A detailed workflow of the steps involved in the bioinformatic analyses is depicted in Supplementary material online, *Figure S5A*.

2.8 3′ untranslated region luciferase reporter assay

Secreted Gaussian luciferase (GL) system was used for the luciferase assay. Briefly, HEK 293 cells (24 well format) were transfected with NS control mimic or miR-369-3p mimic (miRvana) at a concentration of 30 nM for 48 h. Next, cells were transfected with 500 ng of vector only-GL or sucnr1-GL constructs (Genecopeia). At 48-h (total of 96 h) post-transfection, media was collected from the respective cells and luciferase assay was performed following manufacturer's protocol with GL-S buffer. Luciferase activity was measured using the SpectroMax i3× microplate reader luminometer with an integration time of 3 s.

2.9 Quantification of ROS for oxidative stress

At day-6 of BMDM differentiation, cells were harvested and approximately 30 000 cells were seeded in a 96-well plate. Cells were serum-starved overnight followed by treatment with oxLDL or BSA control for 24 h. Cells were also exposed to 10 mM H_2O_2 for 30 min which served as a positive control, while cells that only received PBS served as negative control. After treatment, a dichloro-dihydro-fluorescein diacetate solution (Cat# D399, Invitrogen) was added into each well at a final concentration of 100 μM for 30 min at 37°C and in darkness, as previously described.[34] Intensity of the fluorescence was measured using SpectroMax i3x microplate reader at 490/510 nm (excitation/emission). Data were expressed as the relative mean fluorescence intensity (MFI) and indicated as the ROS level.

2.10 Plasmid transfection in RAW 264.7 macrophages

RAW 264.7 macrophages were plated in a 6-well plate at a seeding density of 0.7×10^6 cells/well. The cells were incubated at 37°C and 5% CO_2 and allowed to adhere to the plate surface. After 4 h, transfection reactions were prepared using 5μg/well DNA from empty vector control (Cat. EX-NEG-M39; Genecopeia) or GPR91/sucnr1 plasmids (Cat. X-MM35267-M39-50; Genecopeia) and lipoplexes were prepared using lipofectamine 2000 (Invitrogen) as per the manufacturer's recommendations. At the time of transfection, the complete medium was removed from the cells and replaced with equal volume of serum-free medium, Opti-MEM® I (Invitrogen). The transfection reactions (lipoplexes) were added directly to the cells and incubated at 37°C in 5% CO_2. After 4 h, an equal transfection volume of complete medium containing 20% serum was added. 48 h after plasmid transfection, the cells were loaded with oxLDL for 24 h, as described above. At the end of the experiment, supernatant was collected for Enzyme-linked immunosorbent assay (ELISA) and cell lysates were prepared for western blot analyses.

2.11 Human study

Adult patients with Type 2 diabetes mellitus (DM), clinically diagnosed coronary artery disease (CAD), Type 2 DM with CAD, and healthy volunteers were recruited at Boston Medical Center by advertisement. Diabetes was defined as fasting glucose ≥126 mg/dL or ongoing treatment for Type 2 DM. Healthy volunteers were taking no medications, had a fasting glucose <100 mg/dL, and had never smoked or had stopped smoking for at least a year prior to enrolment. Supplementary material online, *Table S1* demonstrates the patient characteristics. The study protocol was approved by the Boston Medical Center Institutional Review Board and all participants provided written informed consent in accordance to the Declaration of Helsinki. Venous blood was collected from these patients and processed for isolating PBMCs, as previously described.[35] Total RNA was isolated from human PBMCs stored in RNA protect reagent (Qiagen, Hilden, Germany) by phenol-chloroform method and cleaned-up by miRNeasy micro kit (Qiagen) as per the manufacturer protocol with slight modification. cDNA was synthesized from 200 ng of total RNA including small RNA by using miRCURY LNA RT Kit (Qiagen) on Bio-Rad thermal cycler T100. Quantitative RT–PCR for miR-369-3p gene expression was done by ViiA 7 real time PCR system (Thermo Fisher Scientific) using miRCURY LNA SYBR® Green PCR Kit (Qiagen). Each set of reactions included non-template controls and a melt curve for NS signals. The relative expression of miR-369-3p gene was determined by using internal control RNU6 and calculated as $2^{-\Delta\Delta CT}$.

2.12 Isolation of primary human monocytes from human PBMCs and treatment with GPR91 antagonist

Primary human monocytes were isolated from healthy and diabetic human PBMCs samples using the Pan Monocyte Isolation Kit for human PBMCs (Cat# 130-096-537; Milteny Biotec). Freshly isolated monocytes were

Downloaded from https://academic.oup.com/cardiovascres/advance-article/doi/10.1093/cvr/cvae102/7664626 by Ewha Womans University user on 02 September 2024

incubated with or without 5 μM of NF-56-EJ40 (MedChem Express, HY130246, a potent, highly selective human SUCNR1/GPR91 antagonist) in dimethyl sulfoxide (DMSO) for 30 min followed by oxLDL-treatment for 24 h. Cells treated with DMSO alone served as the control. Supernatants were collected for IL-1β ELISA.

2.13 Animal study

The animal experiments were performed strictly as per the recommendations in the Guide for the Care and Use of Laboratory Animals of the National Institutes of Health. The protocol was approved by the Brigham and Women's Hospital Standing Committee on Animals (2016N000182). Eight to 10-week-old male *Ldlr*−/− mice (C57Bl6 *LDLr*^{tm1Her} from Jackson Laboratories, ME, USA) were placed on HFSC diet for 8 weeks to induce atherosclerosis after which the mice were randomized into two treatment groups ($n = 16$ per group). Mice were anaesthetised with isoflurane/oxygen mixture (2% inhalation) and intravenously injected with 2 nmol of either NS-m control or miR-369-3p mimic (miRvana) biweekly for a total of 4 weeks. At the end of experiment, mice were anaesthetised with 150 μl of a mixture of 20% ketamine/5% xylazine in 0.9% saline through intraperitoneal injection. Once anaesthetised, blood was collected through cardiac puncture followed by perfusion with ice-cold PBS. Mice were euthanized by cervical dislocation under anaesthesia. Aortas were collected for flow cytometry and hearts were embedded in optimal condition temperature and immediately stored in −80°C for future immunohistochemistry. Technical issues during cryosectioning led to exclusion of 2 mice from NS group and 1 mouse from miR-369-3p mimic group. During treatment, 2 mice in the NS and 3 mice in the miR-369-3p mimic group died during retroorbital injection and were excluded from the study.

2.14 Plasma analysis

Plasma was collected at the time of sacrifice by cardiac puncture. Total cholesterol, triglycerides, LDL-C and HDL-C were measured by an enzymatic assay (Thermo Fisher Scientific) at The Lipid Laboratory at the Harvard T.H. Chan School of Public Health (Boston, MA, USA). Non-HDL cholesterol levels were calculated using the following formula: Non-HDL = Total Cholesterol—HDL Cholesterol.

2.15 Glucose and insulin tolerance tests

For glucose tolerance tests (GTTs), mice were fasted for 12 h, and then injected intraperitoneally with d-glucose (Sigma, 1.0 g/kg of body weight). Insulin tolerance tests (ITTs) were performed on mice after 6 h fasting, as we previously reported.[32] Recombinant human regular insulin (0.75 U/kg of body weight, Humulin R, Eli Lilly) was given to mice by intraperitoneal injection. Blood glucose levels were measured before injection and at 15, 30, 60, 90, and 120 min after the administration of glucose or insulin using Contour next EZ blood glucose monitoring system (Bayer).

2.16 Flow cytometry

2.16.1 Aortas

Mice aortas were harvested at the end of the study. Isolated arches were incubated in digestion buffer containing liberase (no. 273582, Roche, Basel, Switzerland), hyaluronidase (no. 3506, Sigma, MO), DNase I (no. DN25, Sigma, MO), and 1 mol/L $CaCl_2$ at 37°C for 15 min using single cell suspension dissociator. The digested tissue was passed through a 70 μm cell strainer, washed with 1× cold PBS and centrifuged at 350 *g* for 10 min at 4°C to get single cell suspensions. For flow cytometry, cells stained with Fixable Viability Dye Zombie yellow orange (Biolegend, San Diego CA, USA) for 30 min on ice, blocked with TruStain fcX (Biolegend) and then stained using PerCP/Cy5.5 anti-mouse CD45, APC anti-mouse Ly6C, APC/Cy7 anti-mouse Ly6G, Pe/Dazzle 594 anti-mouse CD115, PerCP anti-mouse CD11b, BV605 anti-mouse F4/80, AF700 anti-mouse CD11c, BV711 anti-mouse CD206 and PE anti-mouse GPR91 antibody for 30 min on ice. Cells were then fixed and permeabilized in fix-perm wash buffer (BD Biosciences, Franklin Lakes, NJ) for 30 min on ice. The cells were then acquired on Cytek Aurora and analysed with FlowJo V10 (Tree-Star, Ashland, OR). For aortic macrophages sorting, cells were passed through 85 μm nozzle in BD LSR II flow sorter and collected in Qiagen's RNA lysis buffer for further processing.

2.16.2 Blood leukocytes

Blood was withdrawn via tail vein bleeding with Ethylenediaminetetraacetic acid -coated capillary tubes. Red blood cells were lysed with lysis buffer (BD Biosciences) and blocking was achieved with anti-mouse CD16/CD32 (eBioscience). For monocytes and neutrophils, cells were stained with PerCP/Cy5.5 anti-mouse CD45, APC anti-mouse Ly6C, APC/Cy7 anti-mouse Ly6G, Pe/Dazzle 594 anti-mouse CD115. For B cells and T cells markers, cells were stained separately with BV650 anti-mouse CD3, PE-CSF594 anti-mouse CD4, PE/Cy7 anti-mouse CD8, AF647 anti-mouse CD19, PE anti-mouse CD43.

2.17 Isolation of various cell-types for cell-specific profiling of miR-369-3p from atherosclerotic mice

Ldlr−/− mice were placed on HFSC diet for 12 weeks to develop advanced atherosclerosis. Following isolation of aortas and enzymatic digestion, cell suspension was obtained. Isolations of various cell-types was carried out immediately using either flow cytometry-cell sorting (FACS-sorted: macrophages, non-macrophage immune cells, and endothelial cells) or magnetic-activated cell sorting (MACS-sorted: smooth muscle cells and fibroblasts, as we previously described in[36]) In addition, MACS technology was also applied for isolating monocytes and neutrophils from bone marrows of these mice using Miltenyi MACS isolation kits (Cat# 130-100-629 for monocytes and Cat#130-097-658 for neutrophils). Furthermore, PBMCs were isolated from blood of these mice using Lymphocyte Separation Media (LSM; Cat#0916922-CF; MP Biomedicals). For aortic plaques cell sorting, cells were passed through 85 μm nozzle in BD LSR II flow sorter and collected in Trizol LS reagent (Invitrogen) for further processing. MACS-sorted cells as well as PBMCs were lysed with Qiagen's lysis buffer. qPCR analysis was performed of the isolated cells to determine the cell-specific expression of miR-369-3p.

2.18 RNA extraction and reverse transcription quantitative PCR

Total RNA was isolated with the Advanced Cell/Tissue miRNeasy kit (Qiagen) and quantified using Nanodrop 2000 software (Nanodrop Products). Total RNA was isolated from FACS-sorted aortic plaque cells using Direct-zol™ RNA Microprep kit (Zymo Research) and processed for downstream applications. For miR-369-3p expression, cDNA was synthesized from 50–200 ng of total RNA including small RNA by using miRCURY LNA RT Kit (Qiagen) on Bio-Rad thermal cycler T100. Quantitative RT–PCR for miR-369-3p expression was carried on QuantStudio™ 6 Pro (Applied Biosystems) using miRCURY LNA SYBR® Green PCR Kit (Qiagen). The relative expression of miR-369-3p gene was determined by using internal control RNU6 and calculated as $2^{-\Delta\Delta CT}$ (as fold-change) or as $2^{-\Delta CT}$ (as relative expression). For mRNA quantification, cDNA was synthesized using High-Capacity cDNA Reverse Transcription Kit (Thermo Fisher Scientific). Quantitative real-time PCR was performed using GoTaq® qPCR Master Mix (Promega, A6001) on QuantStudio™ 6 Pro (Applied Biosystems). The relative expression of each gene was determined by normalization to hypoxanthine phosphoribosyltransferase as a housekeeping gene and represented as $2^{-\Delta CT}$.

2.19 RNA sequencing and pathway analysis

The total RNA extracted from FACS-sorted aortic macrophages of different mice groups (369-m and NS-m control) were subjected to Ultra-Low Input RNA-Seq (GeneWiz). A SMART-Seq v4 Ultra-Low Input Kit for Sequencing was used for cDNA synthesis and amplification (Clontech, Mountain View CA, USA), and Illumina Nextera XT library was used for sequencing library preparation. Briefly, cDNA was fragmented, and the adaptors were ligated using Transposase. The resulting cDNA fragments

Downloaded from https://academic.oup.com/cardiovascres/advance-article/doi/10.1093/cvr/cvae102/7664626 by Ewha Womans University user on 02 September 2024

were subjected to limited PCR enrichment and index addition prior to the sequencing using an Illumina HiSeq instrument. The sequencing reads were trimmed and mapped to the latest mouse reference genome (Genome Reference Consortium Mouse Build 39). Total gene hit counts and normalized values were calculated for each gene and differential expression analysis (log2 fold-change ≥ 0.58, *P*-adj ≤ 0.1) between specified groups was performed using DESeq2. The core pathway analysis of differentially expressed genes between group 369-m vs. NS control was performed using Ingenuity Pathway Analysis (IPA, Qiagen), and visualization of the pathway enrichment data was performed using R-ggplot2 (version 3.4.3) library. RNA-Seq data are available open access through Gene Expression Omnibus (GSE244760).

2.20 Immunohistochemistry

Hearts were sectioned through the aortic root (6 μm) using a tissue processor (Leica CM3050) and stained with Oil red O (ORO) and haematoxylin and eosin (H&E) for quantification of lesion area, as previously described.[16] The staining area was measured using Image-Pro Plus software (Media Cybernetics).

2.21 Enzyme-linked immunosorbent assay

Cell supernatants were collected from cultured mouse BMDMs as well as from mouse and human primary monocytes. The concentrations of the pro-inflammatory cytokines, IL-1β, TNF-α, and apoptosis-associated speck-like protein (ASC) in the supernatants were detected using ELISA kits (R&D Systems), according to the manufacturer's instruction.

2.22 Multiplex ELISA cytokine profiling

Mouse plasma was collected from each group, aliquoted and stored in −80°C for BMDMs experiments as well as for Cytokine/Chemokine 31-Plex Discovery Assay® Array (MD31, EVE Technologies).

2.23 Statistical analyses

All data are presented as mean ± standard error of the mean (SEM). Data are analysed by GraphPad Prism 9 statistical software (GraphPad Software Inc, San Diego, CA, USA). Comparisons between two groups were analysed by unpaired Student's *t*-test. One-way ANOVA tests were used where indicated followed by Holm-Šídák test for *post hoc* test correction. In case of time-course data for two independent tissue samples, two-way ANOVA with Šidák's multiple comparisons was performed. In Figures, * $P < 0.05$, ** $P < 0.01$, *** $P < 0.001$, and **** $P < 0.0001$ for a given test.

3. Results

3.1 Identification of differentially expressed miRNAs in diabetes-associated atherosclerosis

We first sought to identify the differentially expressed miRNAs in diabetic atherosclerotic plaque progression. *Ldlr*−/− mice were placed on a HFSC diet for 12 weeks to develop advanced atherosclerotic plaques. At this timepoint, RNA was isolated from the intimal layer of lesions and miRNA-seq performed, which revealed differential miRNA expression profiles (log2 fold-change, 1.5; *P*-value <0.05; Supplementary material online, *Figure S1*). Interestingly, miR-369-3p came up as one of the most significantly down-regulated miRNAs in the aortic intima from atherosclerosis progressing mice as compared to chow-diet-fed mice (see Supplementary material online, *Figure S1*). The miRNA-seq results for miR-369-3p were further verified by reverse transcription quantitative PCR (RT-qPCR) which revealed reduced expression of miR-369-3p in the aortic intima after 12 weeks of HFSC diet (progression group) as compared to chow-diet-fed mice (baseline control group) (*Figure 1A*). Importantly, miR-369-3p expression was higher in aortic intima RNA samples (rich in leukocytes and endothelial cells) as compared to media RNA samples (rich in non-immune cells), as shown in *Figure 1A*.

3.2 miR-369-3p expression is enriched in macrophages and is down-regulated in diabetes-associated atherosclerosis

Because the aortic intima is composed of heterogeneous cell-types, we next performed cell-specific profiling of miR-369-3p expression in various cell-types isolated from aortic plaques, bone marrows and PBMCs of *Ldlr*−/− mice fed a HFSC diet for 12 weeks. RT-qPCR analyses of these cell-types revealed a robust enrichment of miR-369-3p in aortic plaque macrophages followed by monocytes and PBMCs (*Figure 1B*). To explore the translational relevance of miR-369-3p in diabetes-associated atherosclerosis, we isolated PBMCs from heathy donors, patients with CAD, DM, or DM with CAD (DM + CAD). miR-369-3p expression was significantly reduced in DM, CAD, and DM + CAD PBMCs (*Figure 1C*). Furthermore, to understand the influence of inflammation on miR-369-3p expression, we determined its expression in response to pro-inflammatory stimuli (Lipopolysaccharide [LPS], oxLDL, palmitate, IL-1β) or anti-inflammatory stimuli (IL-4). miR-369-3p expression was significantly reduced in LPS, IL-1β, palmitate and oxLDL-loaded macrophages (foam cells) compared to unstimulated control macrophages (basal). IL-4 stimulation did not alter miR-369-3p expression compared to basal control (*Figure 1D*). These findings highlight macrophage-enriched expression of miR-369-3p is markedly reduced in response to pro-inflammatory stimuli in mouse BMDMs.

3.3 miR-369-3p overexpression ameliorates oxLDL-mediated metabolic inflammation in BMDMs

miRNAs are important modulators of oxLDL-mediated inflammation in atherosclerosis.[37] miR-369-3p can decrease LPS-mediated intestinal inflammation via regulating BRCC3 expression in BMDMs.[38] However, its role in regulating lipid-driven macrophage inflammation in the context of atherosclerosis is still unknown. Therefore, we sought to determine the specific role of miR-369-3p in regulating macrophage lipid-mediated inflammation. To overexpress miR-369-3p in macrophages, BMDMs were transfected with miR-369-3p mimic (369-m) or NS-m control for 48 h, and subsequently stimulated with oxLDL for 24 h. First, we confirmed the overexpression of miR-369-3p expression by qPCR at both basal and oxLDL-treated conditions (see Supplementary material online, *Figure S2A*). OxLDL-treatment increased the mRNA levels of *Il1b, tnfa, Il6 and nos2* (see Supplementary material online, *Figure S2B–E*) and secretion of pro-inflammatory cytokines (IL-1β and TNF-α) and the NLRP3 inflammasome mediator ASC (apoptosis-associated speck-like protein containing a CARD) (see Supplementary material online, *Figure S2F–H*). Intriguingly, oxLDL-induced *Il1b, tnfa, Il6*, and *nos2 mRNA levels were significantly reduced in* miR-369-3p overexpressing BMDMs. (see Supplementary material online, *Figure S2B–E*). Correspondingly, secretion of pro-inflammatory molecules IL-1β, TNF-α, and ASC was also reduced in miR-369-3p overexpressing BMDMs (see Supplementary material online, *Figure S2F–H*), indicating a crucial role of miR-369-3p in regulating oxLDL-mediated inflammation in macrophages.

3.4 miR-369-3p overexpression restores oxLDL-mediated reduction in mitochondrial respiration and altered cellular metabolites

Altered mitochondrial metabolism results in priming of monocytes and macrophages towards a pro-inflammatory phenotype, characteristic of lesion macrophages.[39,40] Yet, the factors contributing to the skewed macrophage metabolism remain unclear. OxLDL is known to cause mitochondrial dysfunction by generating ROS as well as nitric oxide (NO),[41] and consequently an increase in HIF-1αZ[42] and IL-1β secretion[43] to propagate metabolic inflammation. miR-369-3p has been previously reported to regulate inflammation in bone marrow-derived dendritic cells via decreasing *nos2*.[44] Consistently, our results showed a marked reduction in *il1b* and *nos2* mRNA levels (see Supplementary material online, *Figure S2B and E*) as well as reduced IL-1β secretion in miR-369-3p overexpressing cells despite

Downloaded from https://academic.oup.com/cardiovascres/advance-article/doi/10.1093/cvr/cvae102/7664626 by Ewha Womans University user on 02 September 2024

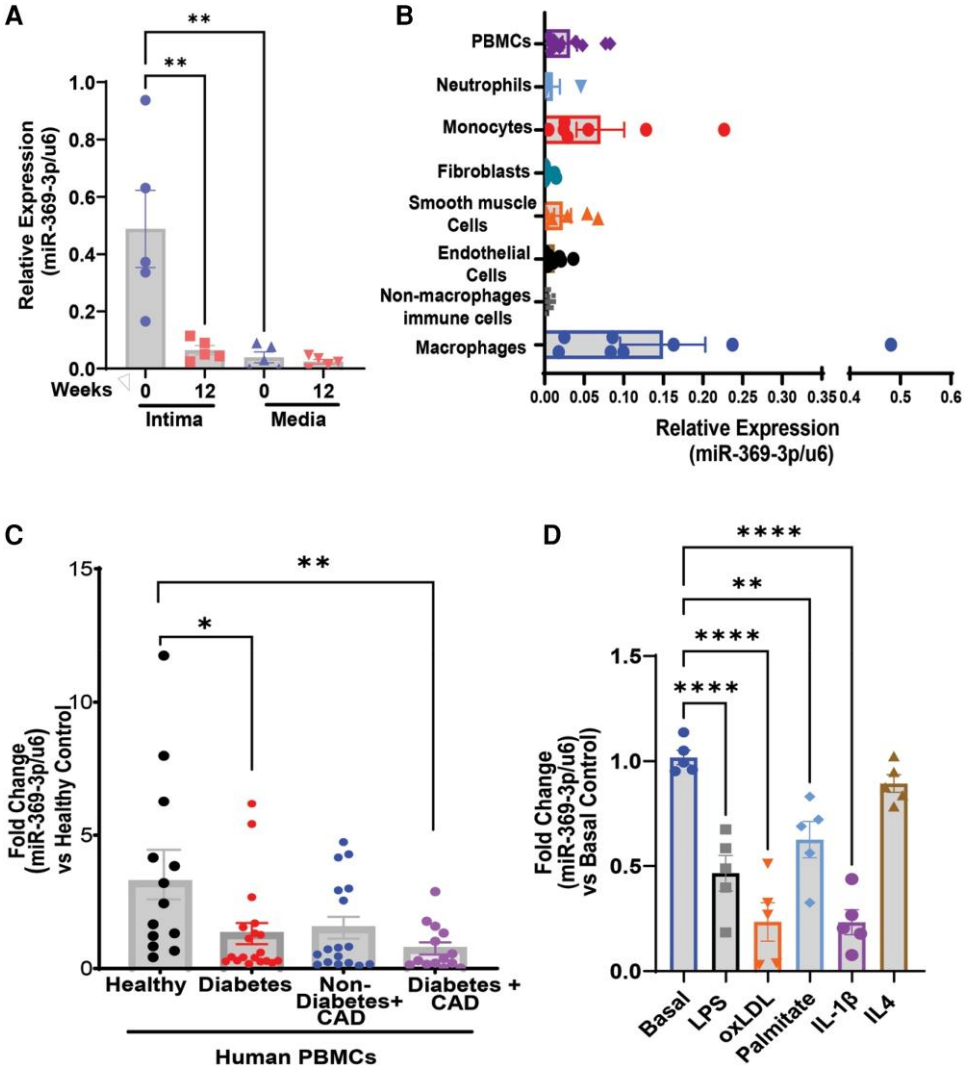

Figure 1 Expression profiling of miR-369-3p expression. (*A*) miR-369-3p expression in aortic intima from *Ldlr*–/– mice on HFSC diet for 12 weeks (progression) or 0 week (chow-diet-fed control); $n = 5$ per group. (*B*) Cell-type profiling of miR-369-3p in FACS-sorted cells (aortic plaque macrophages, non-macrophages immune cells, and endothelial cells); MACs-sorted cells (aortic smooth muscle cells, aortic fibroblasts, primary bone marrow monocytes, and neutrophils); and PBMCs from *Ldlr*–/– mice on HFSC diet for 12 weeks ($N = 7$ mice per group). (*C*) miR-369-3p expression in human PBMCs (healthy controls, DM, CAD, or DM + CAD ($N = 11$–15 subjects/group). (*D*) miR-369-3p expression in BMDMs under the various indicated stimuli or basal control ($N = 5$ biological replicates per group). BMDMs were stimulated with Lipopolysaccharide (LPS) (50 ng/mL); oxLDL (50 μg/mL); palmitate (200 μM); IL-1β (10 ng/mL), or IL-4 (10 ng/mL). Unstimulated BMDMs (Basal) were used as control. Statistical analyses were performed using two-way ANOVA followed by Šídák's test for multiple comparisons (*A*) or using one-way ANOVA followed by Holm-Šídák test for multiple comparisons (*C* and *D*). All data are mean ± SEM. Statistical differences are indicated as $*P < 0.05$; $**P < 0.01$, $***P < 0.001$, and $****P < 0.001$ vs. control.

stimulation by oxLDL (see Supplementary material online, *Figure S2F*). Thus, we speculated if miR-369-3p plays a direct role in regulating oxLDL-induced metabolic reprogramming. To explore this in further detail, Seahorse assay was performed to assess mitochondrial respiration in BMDMs loaded with oxLDL with or without miR-369-3p overexpression. OxLDL-treated macrophages with NS-m control were distinguishable by a decreased OCR, as evident by a decrease in basal and maximal respiration, ATP production, and an increase in proton leak (*Figure 2A and B*). In contrast, these oxLDL-treated macrophages exhibited an increased ECAR as evident by an increase in glycolytic capacity (*Figure 2C and D*), signifying enhanced glycolytic flux in these cells. In addition to decreased OCR, we observed concurrent downregulation of oxidative phosphorylation (OXPHOS) complexes (*Figure 2E and F*) in oxLDL-loaded macrophages. These findings indicated that oxLDL-treated macrophages preferentially use aerobic glycolysis over OXPHOS, contributing to a pro-inflammatory phenotype. Importantly, overexpressing miR-369-3p reversed these effects (*Figure 2A–D*) and promoted OXPHOS (OCR) for energy production over glycolysis (ECAR), suggestive of an anti-inflammatory phenotype. We also found that the oxLDL-mediated decrease in OXPHOS subunits was restored by miR-369-3p overexpression (*Figure 2E and F*).

OxLDL is known to shift cellular energy balance to a glycolytic profile through generation of ROS and stabilizing HIF-1α protein levels which increases inflammatory cytokine secretion, specifically, IL-1β.[45,46] These metabolic impairments have been recently shown to be associated with dysregulation of cellular metabolites in human macrophages. Because oxLDL-loaded miR-369-3p overexpressing BMDMs restored mitochondrial

Downloaded from https://academic.oup.com/cardiovascres/advance-article/doi/10.1093/cvr/cvae102/7664626 by Ewha Womans University user on 02 September 2024

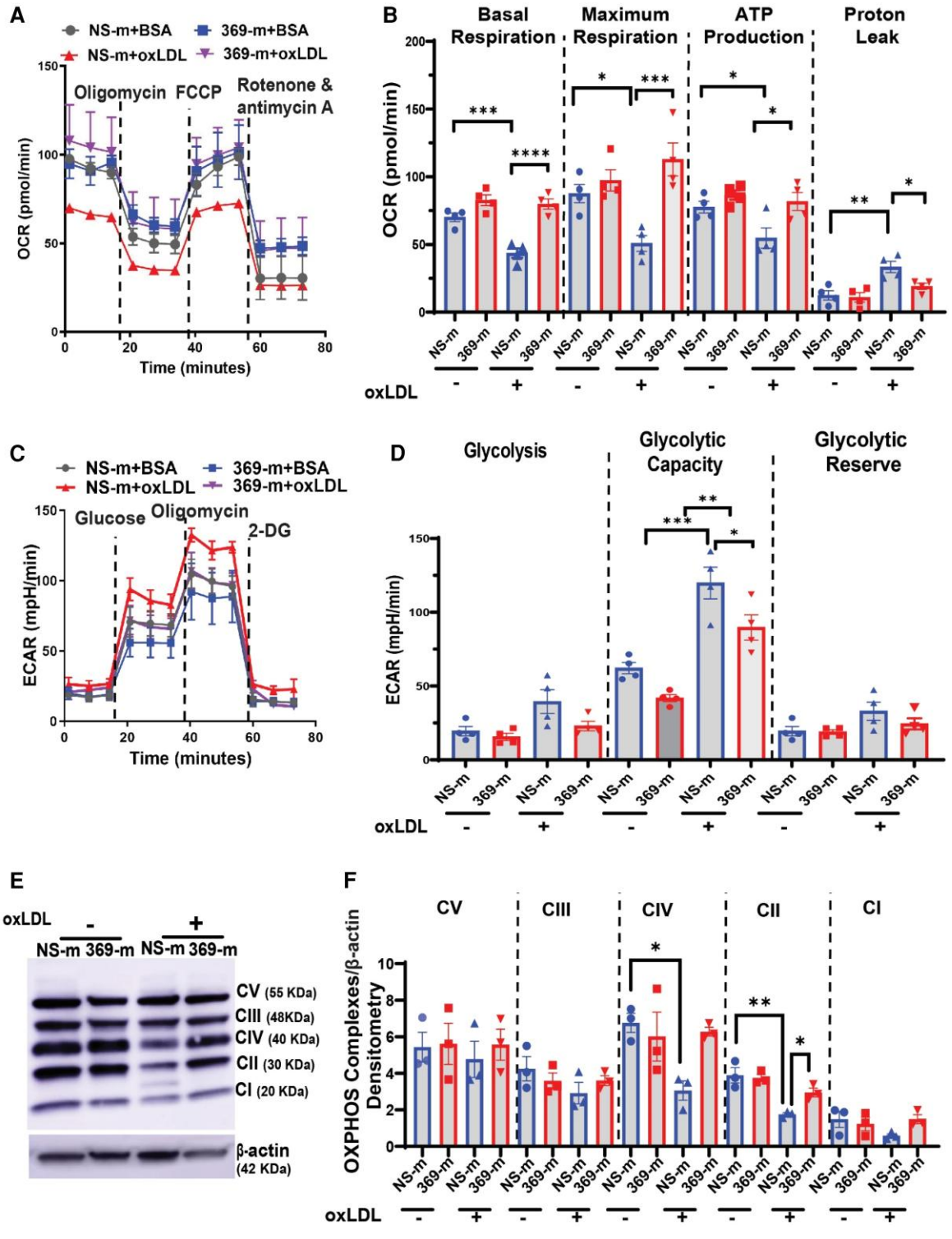

Figure 2 miR-369-3p overexpression in BMDMs reduces oxLDL-mediated mitochondrial stress pro-inflammatory mediators. BMDMs were transfected with NS-m control or miR-369-3p (369-m) mimic (30 nM) for 48 h, after which the cells were serum-starved overnight and oxLDL was loaded for 24 h. (*A–D*) Seahorse analysis of cellular (*A* and *B*) OCR, basal respiration, maximum respiration, and spare respiratory capacity, (*C* and *D*) ECAR, glycolysis, glycolytic capacity, and glycolytic reserve. Data are normalized to total protein content and expressed as mean ± SEM ($N = 4$ biological replicates per group). (*E* and *F*) Western blotting was performed on total cell lysates to determine the levels of OXPHOS complex ($N = 3$ biological replicates per group). Statistical analysis was performed using one-way ANOVA followed by Holm-Šídák test for multiple comparisons. All data are mean ± SEM. Statistical differences are indicated as $^{*}P < 0.05$; $^{**}P < 0.01$; $^{***}P < 0.001$; and $^{****}P < 0.0001$ vs. NS-m control.

Downloaded from https://academic.oup.com/cardiovascres/advance-article/doi/10.1093/cvr/cvae102/7664626 by Ewha Womans University user on 02 September 2024

homeostasis (*Figure 2A and B*) and reduced IL-1β secretion (see Supplementary material online, *Figure S1E*), we speculated that miR-369-3p may play a critical role in regulating oxLDL-mediated metabolic reprogramming by modulating the levels of specific cellular metabolites. To characterize the metabolic reprogramming in macrophages, we performed metabolomics analyses in the supernatants from oxLDL-treated BMDMs with or without miR-369-3p overexpression and determined the extracellular metabolic profile under these conditions. Consistent with the increase in pro-inflammatory cytokine secretion, the levels of about 20 extracellular metabolites also changed substantially after oxLDL-loading in macrophages vs. BSA control (*Figure 3A*). OxLDL-stimulated macrophages exhibited altered patterns of some key metabolites (*Figure 3B*). Among the most profound alterations in metabolites was the increase in succinate levels (*Figure3B*), which was found to be associated with several metabolic pathways, including the citric acid (TCA) cycle (*Figure 3C*). As an intermediate of the TCA cycle, succinate is released and accumulates under hypoxia and oxidative stress to promote glycolysis and the Warburg effect.[11,14] Overexpression of miR-369-3p in oxLDL-loaded BMDMs showed a markedly different pattern of extracellular metabolites compared to the NS control group in oxLDL-loaded BMDMs (*Figure 3B*), including reduced extracellular release of succinate. These observations were further validated by a colorimetric assay for measuring succinate (*Figure 3D*). Next, to understand the functional relevance of increased extracellular succinate, we isolated monocytes from C57BL6 mice and treated them with either succinate alone or primed them with succinate prior to oxLDL-treatment. As shown in Supplementary material online, *Figure S3A–C*, oxLDL alone increased the activation of monocytes, indicated by an increase in percentage of $Ly6C^{hi}$ pro-inflammatory monocyte subset and a decrease in the $Ly6C^{lo}$ anti-inflammatory subset. While succinate alone has no effect on the activation of monocytes, priming of monocytes with succinate prior to oxLDL-treatment enhanced the pro-inflammatory phenotype in monocytes (see Supplementary material online, *Figure S3B*). In addition to an increase in the $Ly6C^{hi}$ subset, there was a significant increase in IL-1β secretion in oxLDL-loaded monocytes as well as those primed with succinate prior to oxLDL-treatment (see Supplementary material online, *Figure S3D*).

An increase in intracellular succinate levels have been previously shown to promote IL-1β transcription via stabilization of HIF-1α after LPS stimulation.[14,47] Elevated cytosolic succinate levels may promote protein post-translational modifications by addition of succinyl groups to a lysine residue of a protein.[48] Notably, we found that oxLDL-stimulated BMDMs also showed significantly increased levels of intracellular succinate, which was coupled with an increase in HIF-1α protein expression. Interestingly, these effects were attenuated in miR-369-3p overexpressing (369-m) BMDMs (see Supplementary material online, *Figure S4A–C*). Therefore, to examine if oxLDL-mediated succinate accumulation is directly involved in regulating HIF1α expression in BMDMs, we incubated BMDMs with DMM prior to oxLDL-treatment. DMM is a SDH inhibitor that is known to reduce succinate accumulation.[49] While oxLDL-loading alone increased HIF-1α protein, pre-treating oxLDL-stimulating BMDMs with DMM effectively reduced HIF-1α protein expression (see Supplementary material online, *Figure S4D and E*), indicating that the reduction in HIF-1α expression in oxLDL-loaded BMDMs upon miR-369-3p overexpression (see Supplementary material online, *Figure S4B and C*) was likely due to decreased succinate accumulation by miR-369-3p. Together, these results highlight that: (i) oxLDL-stimulated BMDMs exhibit an increase in extracellular and intracellular succinate levels to drive inflammation in macrophages; and (ii) miR-369-3p overexpression ameliorated the oxLDL-mediated metabolic inflammation in macrophages.

3.5 Identification of GPR91 as a target of miR-369-3p

To understand the molecular mechanisms by which miR-369-3p regulated oxLDL-mediated metabolic inflammation, we sought to determine its targets. We used TargetScan database to perform bioinformatic analysis to predict miR-369-3p targets that have a putative seed region for miR-369-3p binding in their 3′-UTRs (untranslated region). Our bioinformatic analysis predicted a total of 303 putative targets that were common between mouse and human species (see Supplementary material online, *Figure S5A*). Using GO enrichment analyses, we identified target genes that were associated with inflammation (GO: 0050727). This led to identifying seven putative target genes associated with regulation of inflammatory response (*sucnr1*, *cebpb*, *metrnl*, *adipoq*, *stap1*, *il22*, and *hgf*) (see Supplementary material online, *Figure S5A*). Our metabolomics data showed an increase in succinate levels in oxLDL-loaded BMDMs (*Figure 3B*). Intriguingly, succinate is known to bind to its cognate receptor SUCNR1 (also known as GPR91) and activates its signalling to propagate inflammation in macrophages under diabetes[50] and diet-induced obesity.[51] Thus, we hypothesized that SUCNR1 may play a role in driving the oxLDL-mediated metabolic inflammation and may underlie the ability of miR-369-3p to confer anti-inflammatory effects via regulating GPR91 expression. To further confirm this, we performed 3′ UTR luciferase reporter assays and found that miR-369-3p overexpression repressed the wild-type GPR91 3′ UTR compared to the NS control (see Supplementary material online, *Figure S5B and C*). In contrast, there was no change in 3′ UTR reporter activity using a GPR91 3′ UTR harbouring a mutant seed region in the presence of miR-369-3p (see Supplementary material online, *Figure S5B and C*), indicating GPR91 is a direct target of miR-369-3p.

3.6 miR-369-3p overexpression abrogated the succinate-GPR91 signalling in oxLDL-treated BMDMs

In response to inflammatory signals, succinate is released in the extracellular milieu and can bind to and activate its cognate receptor, GPR91 (SUCNR1)[52,53] which then acts in synergy with toll-like receptors to propagate inflammation.[34] GPR91 is a G-protein coupled receptor that acts as a cell surface sensor for extracellular succinate and is known to play a critical role in mediating metabolic reprogramming in dendritic cells, endothelial cells, and macrophages. Analyses of metabolites of the supernatants revealed that oxLDL elicited the release of succinate along with several other inflammatory metabolites from macrophages, while miR-369-3p overexpression abrogated this effect (*Figure 3A, B, and D*). In addition, oxLDL-treated macrophages showed increased GPR91 expression, suggesting that activation of the succinate-GPR91 signalling may contribute at least in part to the oxLDL-mediated inflammation (*Figure 4A and B*). In contrast, miR-369-3p overexpression repressed the expression of GPR91 in oxLDL-loaded macrophages (*Figure 4A and B*).

GPR91 plays an important role in inflammasome activation in chronic inflammatory diseases, such as diabetic kidney disease.[51,54–58] Therefore, we next assessed the components of the inflammasome pathway (NLRP3, cleaved caspase 1 and cleaved IL-1β) in oxLDL-treated macrophages. We observed a significant increase in these inflammasome mediators parallel to the upregulation of GPR91, whereas overexpression of miR-369-3p ameliorated GPR91-mediated inflammasome activation (*Figure4A, C, F, and G*) in oxLDL-treated macrophages. OxLDL-mediated ROS generation is a consequence of mitochondrial dysfunction which subsequently results in inflammasome activation.[45,46] GPR91 was shown to facilitate mitochondrial dysfunction in cardiomyocytes by activating extracellular signal-regulated kinases (ERK) signalling (*P*-ERK 1/2) and its downstream mediator Drp1 (p-Drp1) under the hypoxic state.[59] In another study, p-DRP1 activation was shown to increase the ROS production and subsequently increase the NLRP3 inflammasome.[60] To further investigate if overexpression of miR-369-3p in oxLDL-treated BMDMs regulates the mitochondrial dynamics via the succinate-GPR91 signalling pathway, we investigated p-ERK and p-Drp1 levels in oxLDL-treated macrophages. p-Drp1 is known to promote mitochondrial fission under metabolic stress conditions.[61,62] While p-ERK1/2 and p-DRP1 expression were up-regulated in oxLDL-loaded BMDMs, miR-369-3p overexpression blocked this induction (*Figure 4A, D, and E*). Taken together, these findings suggest that miR-369-3p dampens oxLDL-mediated mitochondrial dysfunction and inflammasome activation at least, in part, through the regulation of the succinate-GPR91 pathway.

3.7 GPR91 is up-regulated in oxLDL-treated macrophages in a ROS-dependent manner

The above findings suggested that GPR91 is up-regulated in response to oxLDL, while miR-369-3p repressed its expression and altered macrophage

Downloaded from https://academic.oup.com/cardiovascres/advance-article/doi/10.1093/cvr/cvae102/7664626 by Ewha Womans University user on 02 September 2024

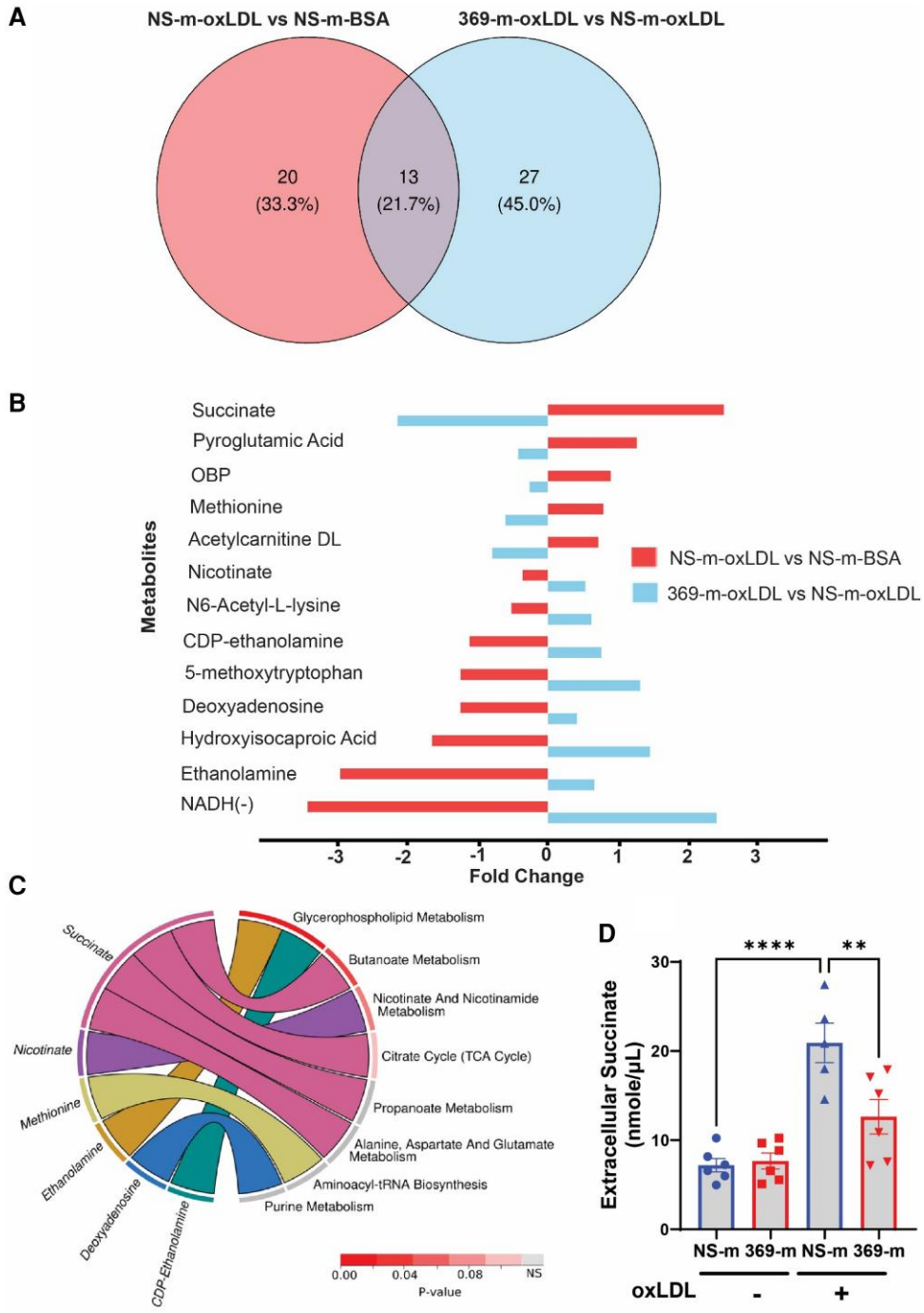

Figure 3 Effect of miR-369-3p overexpression alters global extracellular metabolic profile in oxLDL-treated BMDMs. (*A*) Venn diagram displaying altered metabolites between NS-m-oxLDL vs. NS-m-BSA and 369-m-oxLDL vs. NS-m-oxLDL ($N = 3$ biological replicates per group). (*B*) Bar plot showing 13 common altered metabolites between NS-m-oxLDL vs. NS-m-BSA and 369-m-oxLDL vs. NS-m-oxLDL. (*C*) Chordplot for metabolic pathways associated with altered metabolites that are inversely regulated between (NS-m-oxLDL vs. NS-m-BSA) and (369-m-oxLDL vs. NS-m-oxLDL) using the KEGG database and metaboanalyst tool (v5). *P*-values were generated by metaboanalyst tool based on the number of metabolites associated per pathway (*D*) Validation of extracellular succinate levels by colorimetric assay in oxLDL-treated BMDMs with or without miR-369-3p overexpression. Statistical analysis was performed using one-way ANOVA followed by Holm-Šídák test for multiple comparisons. All data are mean ± SEM. Statistical differences are indicated as $^{**}P < 0.01$ and $^{****}P < 0.0001$ vs. NS-m control.

cellular energetics. However, it remains unclear how GPR91 is regulated under oxLDL stimulation. OxLDL is known to induce persistent ROS production which in turn, regulates the expression of several pro-inflammatory genes.[63,64] Therefore, we investigated if oxLDL-mediated ROS generation up-regulates GPR91 expression and activates downstream NLRP3 inflammasome expression in BMDMs. We first confirmed the increased levels of cellular ROS in oxLDL-loaded BMDMs. In contrast, pre-treatment with NAC, a ROS inhibitor, significantly reduced the oxLDL-mediated ROS generation

Downloaded from https://academic.oup.com/cardiovascres/advance-article/doi/10.1093/cvr/cvae102/7664626 by Ewha Womans University user on 02 September 2024

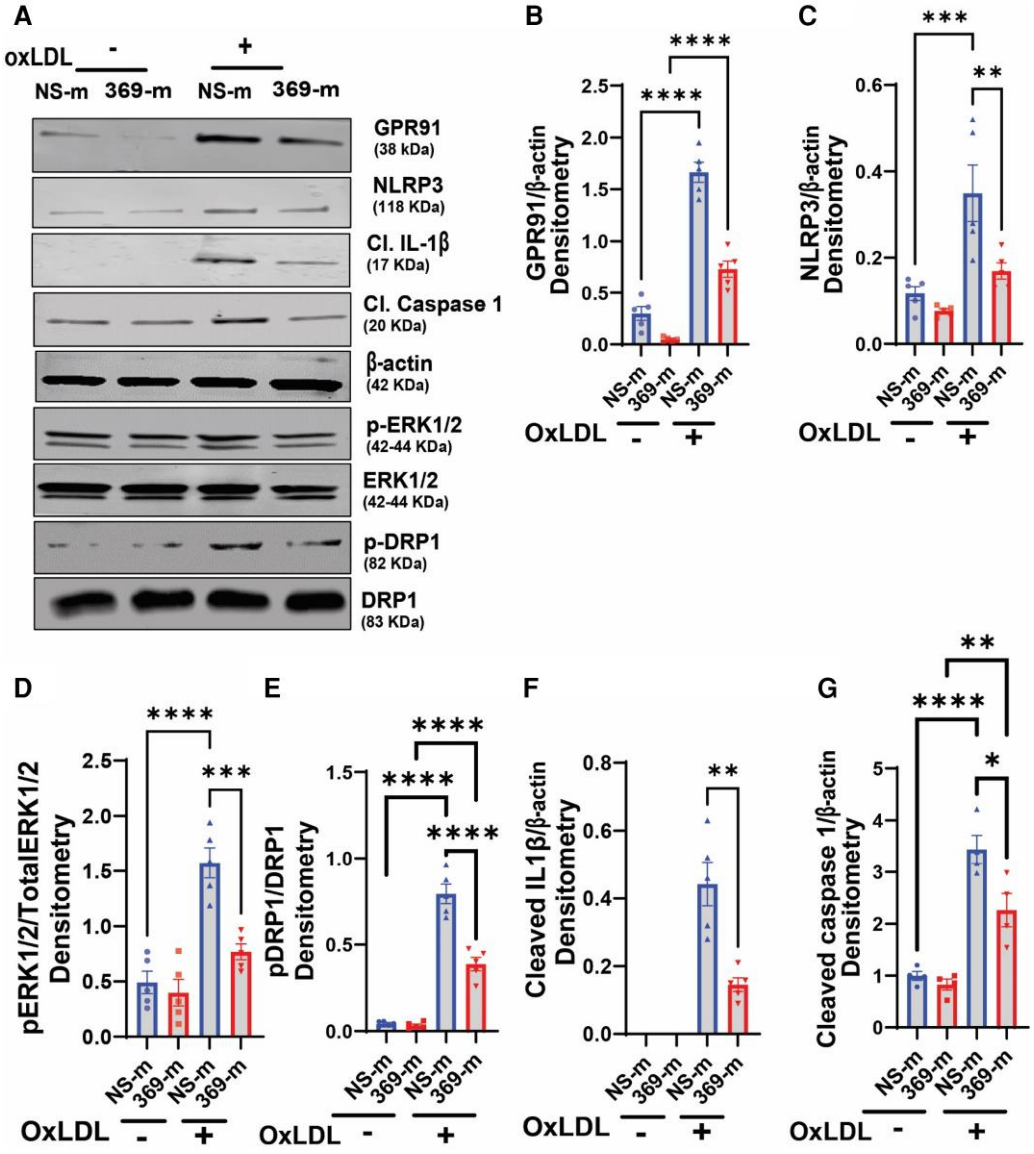

Figure 4 miR-369-3p regulates GPR91-mediated inflammasome activation and mitochondrial dysfunction markers in oxLDL-loaded macrophages. (*A–G*) BMDMs were transfected with NS-m control or miR-369-3p (369-m) mimic (30 nM) for 48 h, after which the cells were serum-starved overnight and oxLDL was loaded for 24 h. Whole cell lysate was prepared, and western blotting was performed. Representative blots (*A*) and quantification of western blots for GPR91 (*B*), NLRP3 (*C*), phosphor-ERK1/2 (*D*), phospho-DRP1 (*E*), cleaved IL-1β (*F*), and cleaved caspase 1 (*G*) using ImageJ software ($N = 5$ biological replicates per group). Statistical analysis was performed using one-way ANOVA followed by Holm-Šídák test for multiple comparisons. All data are mean ± SEM. Statistical differences are indicated as $^{*}P < 0.05$; $^{**}P < 0.01$; $^{***}P < 0.001$; and $^{****}P < 0.0001$ vs. NS-m control.

(see Supplementary material online, *Figure S6A*). Using the same experimental conditions, we next assessed the protein expression of GPR91 and NLRP3 with and without NAC pre-treatment. Strikingly, NAC treatment markedly reduced the oxLDL-mediated induction of GPR91 and NLRP3 expression (see Supplementary material online, *Figure S6B*), suggesting that oxLDL-mediated ROS generation up-regulates GPR91 expression.

3.8 Inhibition of miR-369-3p increases GPR91 expression and contributes to oxLDL-mediated inflammation in BMDMs

Because miR-369-3p overexpression conferred protective effects on oxLDL-mediated mitochondrial inflammation and metabolic dysfunction, we also explored the impact of miR-369-3p inhibition. BMDMs were treated with miR-369-3p inhibitor or NS inhibitor control, followed by oxLDL-loading. As expected, miR-369-3p inhibition resulted in a profound increase in GPR91 expression in oxLDL-loaded BMDMs (see Supplementary material online, *Figure S7A and B*). Examination of inflammasome mediators revealed that miR-369-3p inhibition increased NLRP3 and cleaved IL-1β in oxLDL-loaded BMDMs (see Supplementary material online, *Figure S7A, C, and D*). Furthermore, miR-369-3p inhibition also increased the downstream activation of p-ERK1 (see Supplementary material online, *Figure S7A and E*) and p-DRP1 (see Supplementary material online, *Figure S7A and F*) that are involved in mitochondrial dysfunction. Correspondingly, OXPHOS subunits, CIV and CII were also down-regulated upon miR-369-3p inhibition (see Supplementary material online, *Figure S7G and H*). These findings further support our data that miR-369-3p is critical in the maintenance of mitochondrial homeostasis and regulation of metabolic inflammation.

Downloaded from https://academic.oup.com/cardiovascres/advance-article/doi/10.1093/cvr/cvae102/7664626 by Ewha Womans University user on 02 September 2024

We next assessed if the functional changes in macrophage inflammation after miR-369-3p inhibition are directly attributed to GPR91. Firstly, using mouse macrophage RAW 264.7 cells, we overexpressed GPR91 followed by treatment with BSA control or oxLDL for 24 h. Western blot analyses confirmed the overexpression of GPR91 with or without oxLDL-loaded Raw 264.7 cells, as shown in Supplementary material online, *Figure S8A and B*. Further, it was observed that GPR91 overexpression increased NLRP3 (see Supplementary material online, *Figure S8A and C*) and IL-1β release (see Supplementary material online, *Figure S8D*), suggesting GPR91 acts upstream of activation of inflammasome pathway. To further corroborate our findings, BMDMs were treated with control siRNA NS control inhibitor, GPR91-specific siRNA, miR-369-3p inhibitor, or a combination of GPR91 siRNA and miR-369-3p inhibitor, followed by oxLDL-treatment for 24 h (*Figure 5A–E*). Our results showed that the oxLDL-mediated increase in succinate paralleled an increase in GPR91, NLRP3, and IL-1β (*Figure 5A–E*). Further, these changes were significantly higher in the presence of miR-369-3p inhibitor. In response to siRNA-mediated knockdown of GPR91, the oxLDL-mediated NLRP3 induction was significantly reduced. Intriguingly, using the miR-369-3p inhibitor in the presence of GPR91 siRNA showed a lower induction in NLRP3 expression and IL-1β secretion, indicating a direct role of miR-369-3p in regulating GPR91 and in turn NLRP3-mediated inflammation in macrophages. Notably, inhibition of miR-369-3p increased the release of extracellular succinate (*Figure 5E*). However, using GPR91 siRNA either in the presence or absence of miR-369-3p inhibitor did not significantly alter the levels of succinate in oxLDL-treated BMDMs (*Figure 5E*), suggesting that the miR-369-3p regulation on succinate extracellular release may be independent of GPR91 expression. Future studies will be of interest to clarify the GPR91-mediated effects on succinate extracellular release.

3.9 miR-369-3p overexpression *in vivo* inhibits GPR91 expression, inflammasome activation, and diabetes-associated atherosclerosis

Because overexpression of miR-369-3p *in vitro* dampened metabolic inflammation, we sought to determine the therapeutic potential of miR-369-3p in diabetes-associated atherosclerosis. *Ldlr−/−* mice were fed a HFSC for 8 weeks to develop plaques, following which miR-369-3p mimic (369-m) or NS-m control were administered for 4 weeks (*Figure6A*). qPCR analysis on FACS-sorted aortic macrophages showed ~7-fold increase in miR-369-3p expression in the 369-m group compared to NS control (*Figure 6B*). Furthermore, miR-369-3p administration reduced atherosclerotic lesion size by 27% (*Figure 6C and D*) and ORO lipid content by 25% in the aortic sinus when compared to NS control (*Figure 6C and E*). No significant changes were observed in the GTT, ITT, body weight, blood glucose, and the lipid profile in both groups (see Supplementary material online, *Figure S9A–H*).

Using mRNA-Seq and miR-Seq analyses from the intimal layer of Ldlr−/− mice, we observed a marked reduction in miR-369-3p expression (see Supplementary material online, *Figure S10A*) and a parallel increase in GPR91/sucnr1 expression (see Supplementary material online, *Figure S10B*) with the atherosclerosis progression. Correlation analyses revealed an inverse correlation ($r = -81$; $P < 0.05$) between the expression of miR-369-3p and GPR91 at baseline (chow-diet) and advanced stages (12 weeks HFSC diet) of diabetic atherosclerosis progression (see Supplementary material online, *Figure S10A–C*). To assess the cell-specific expression of GPR91 in the atherosclerosis lesions, we performed immunophenotyping of GPR91 on whole aortas derived from *Ldlr−/−* mice with advanced lesions using flow cytometry. We observed GPR91 to be highly expressed in aortic plaque macrophages and infiltrating monocytes, as measured by MFI (see Supplementary material online, *Figure S10D*). Intriguingly, therapeutic delivery of miR-369-3p mimics (369-m) in HFSC-fed LDLR−/− mice significantly reduced GPR91 expression compared to NS control injected mice (see Supplementary material online, *Figure S10E*). Collectively, these results highlight that (i) the progression of diabetes-associated atherosclerosis leads to a decrease in miR-369-3p and an increase in GPR91 expression in lesions; and (ii) restoration of miR-369-3p expression in aortic plaque macrophages markedly repressed GPR91 expression and lesion formation.

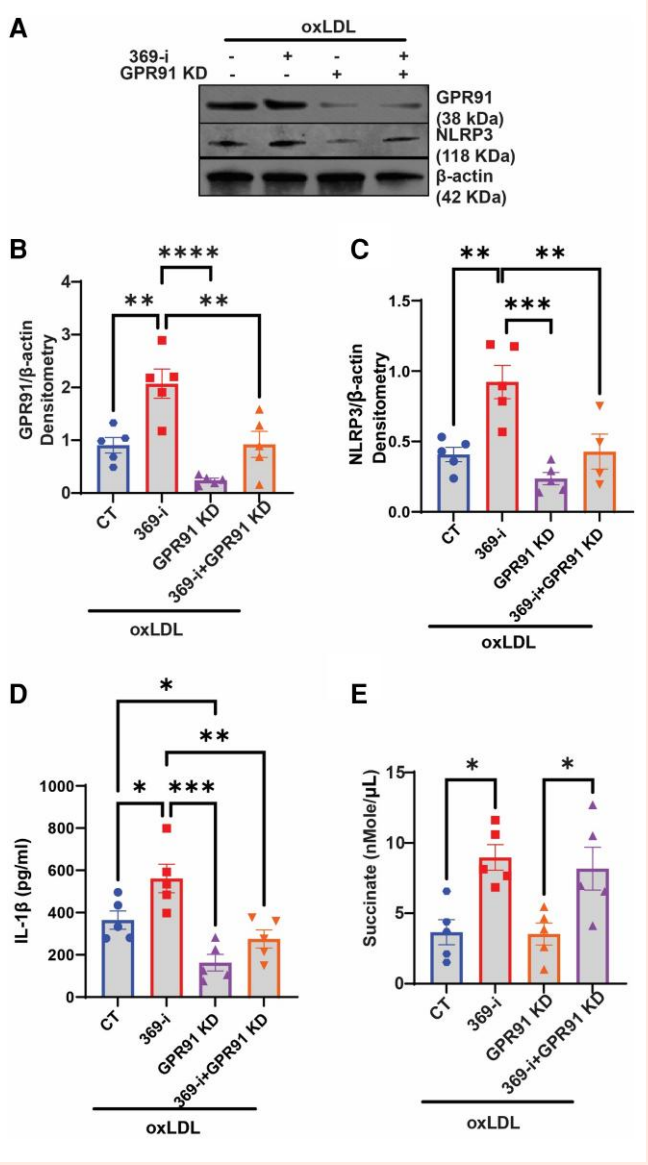

Figure 5 oxLDL-mediated inflammation is exacerbated by miR-369-3p inhibition and is partially dependent on GPR91 in macrophages. BMDMs were transfected with NS inhibitor/siRNA control (CT) or miR-369-3p inhibitor (369-i), or GPR91 siRNA (GPR91 KD) or co-transfected with both 369-i and GPR91 KD for 72 h, after which the cells were serum-starved overnight and oxLDL was loaded for 24 h. Whole cell lysate was prepared, and western blotting was performed. Representative blots (*A*) and quantification of western blots for GPR91 (*B*) and NLRP3 (*C*) are shown. ELISA was performed on cell supernatants to detect IL-1β (*D*). Extracellular succinate levels were measured by colorimetric assay (*E*). $N = 5$ biological replicates per group for all experiments. Statistical analysis was performed using one-way ANOVA followed by Holm-Šídák test for multiple comparisons. All data are mean ± SEM. Statistical differences are indicated as $^{*}P < 0.05$; $^{**}P < 0.01$; $^{***}P < 0.001$; and $^{****}P < 0.0001$ vs. NS-m control.

RNA-Seq analyses of FACS-sorted aortic macrophages from NS-m and 369-m-injected mice revealed a marked downregulation of sucnr1

Downloaded from https://academic.oup.com/cardiovascres/advance-article/doi/10.1093/cvr/cvae102/7664626 by Ewha Womans University user on 02 September 2024

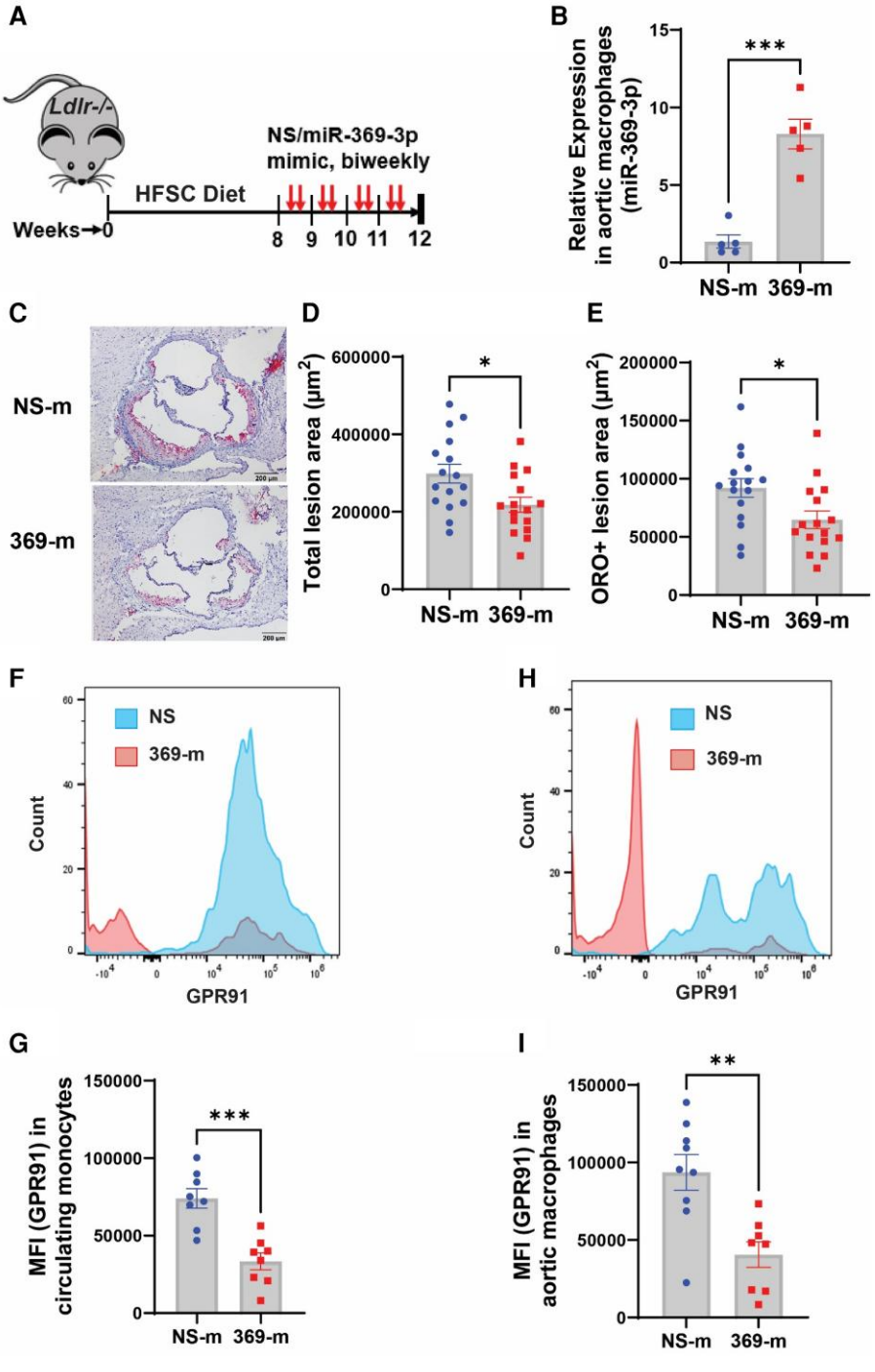

Figure 6 *In vivo* miR-369-3p overexpression halts diabetes-associated atherosclerosis progression (*A*) experimental outline: diabetes-associated atherosclerosis was established in Ldlr−/− mice by feeding a HFSC diet for 8 weeks after which mice were treated with NS-m control or miR-369-3p mimic (369-m) for 4 weeks on HFSC. (*B*) Cells were FACS-sorted directly into Trizol LS for lysis and total RNA was isolated to assess miR-369-3p expression using RT-qPCR analyses ($N = 5$/group). (*C–E*) Representative images (*C*) and quantification of aortic sinus lesion size (*D*) and lipid content (*E*) using ORO staining ($N = 16$ mice per group) are shown. Scale bar = 200 μm. (*F–I*) GPR91 expression was quantified as MFI in circulating monocytes (*F* and *G*) and aortic arch macrophages (*H* and *I*) using flow cytometry analyses ($N = 8–9$ mice per group). All data are mean ± SEM. Statistical analysis was performed using unpaired Student's *t*-test and statistical differences were indicated as $^{*}P < 0.05$; $^{**}P < 0.01$; and $^{***}P < 0.001$ vs. NS-m control.

(GPR91) in the 369-m-injected mice compared to NS-m control mice (see Supplementary material online, *Figure S11A*). Correspondingly, flow cytometric analyses revealed a reduction of GPR91 in both circulating monocytes (*Figure 6E and F*) and aortic macrophages in 369-m-injected-injected mice compared to the NS-m group (*Figure 6G and H*). Furthermore, miR-369-3p restoration decreased CD68+ macrophage content (*Figure 7A and B*) and macrophage NLRP3 expression in aortic lesions in the miR-369-m treated group as compared to the NS control

Downloaded from https://academic.oup.com/cardiovascres/advance-article/doi/10.1093/cvr/cvae102/7664626 by Ewha Womans University user on 02 September 2024

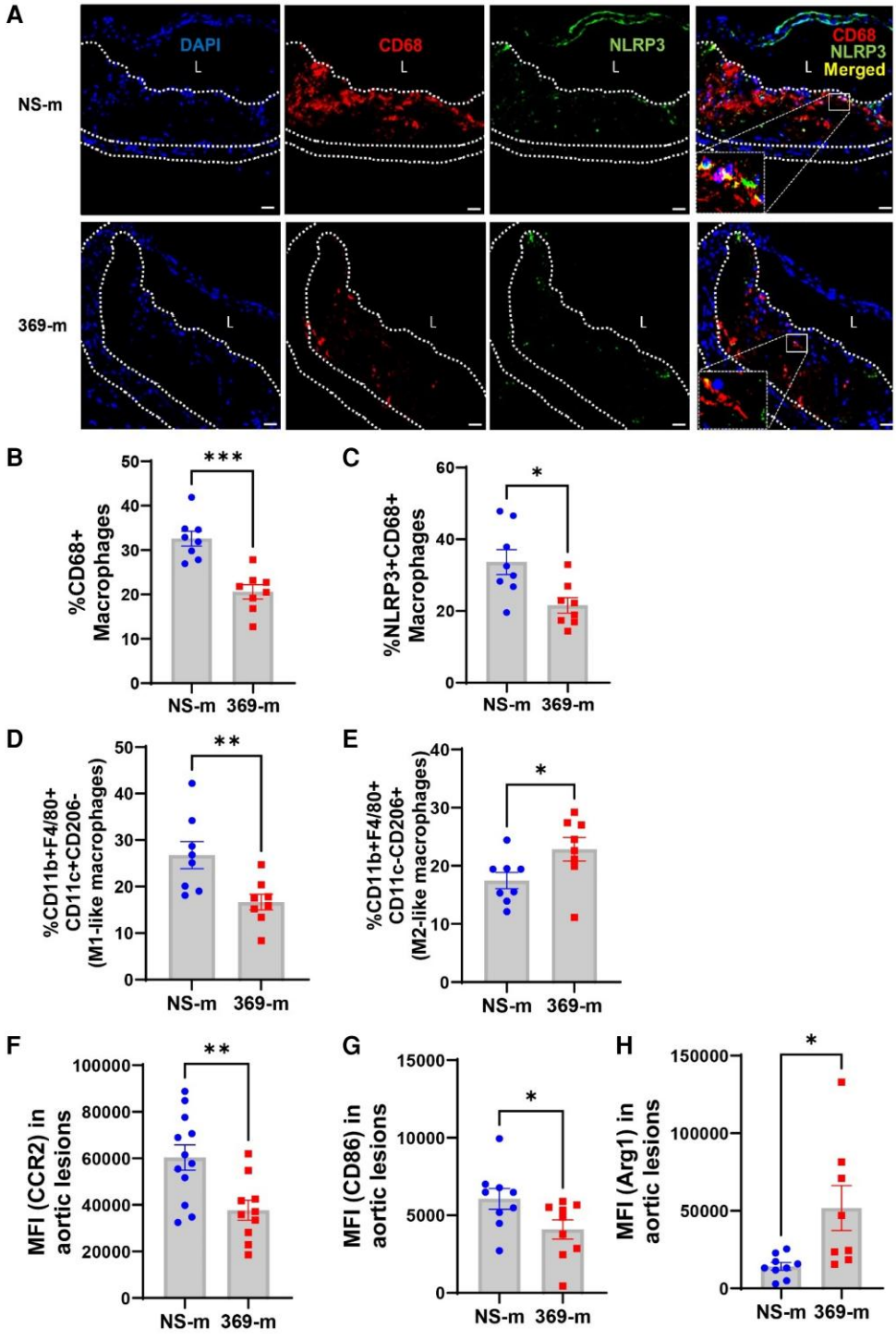

Figure 7 Therapeutic delivery of miR-369-3p reduced the expression of NLRP3 inflammasome in plaque macrophages and is associated with accumulation of alternatively active macrophages M2-like macrophages in the aortic plaques. (*A*) Shown are representative images and (*B*) quantification of CD68+ macrophages and (*C*) NLRP3+CD68+ macrophage staining in the aortic lesions of *Ldlr*−/− mice treated with miR-369-3p mimic (369-m) or NS-m control ($N = 8$ per group; scale bar = 50 μm). (*D* and *E*) Flow cytometric analyses of % M1 (*B*) and % M2 (*C*) subsets of CD11b + F4/80 + infiltrated macrophages ($N = 8$–9 mice per group). (*F*–*H*) Flow cytometric analyses of pro-inflammatory M1 markers, CCR2 (*F*), CD86 (*G*) and anti-inflammatory M2 marker, Arg1 (*H*). All data are mean ± SEM. Statistical analysis was performed using unpaired Student's *t*-test and statistical differences were indicated as $^{*}P < 0.05$; $^{**}P < 0.01$; and $^{***}P < 0.001$ vs. NS-m control.

group (*Figure 7A and C*). The circulating levels of IL-1β (see Supplementary material online, *Figure S12A*) and other inflammatory markers such as LIF (see Supplementary material online, *Figure S12D*) and CCL3 (see Supplementary material online, *Figure S12C*) were reduced in the miR-369-m treated group with non-significant trends for lower levels of TNF-α (see Supplementary material online, *Figure S12E*), IL-6 (see

Downloaded from https://academic.oup.com/cardiovascres/advance-article/doi/10.1093/cvr/cvae102/7664626 by Ewha Womans University user on 02 September 2024

Supplementary material online, *Figure S12F*), MCP-1 (see Supplementary material online, *Figure S12G*), and CXCL1 (see Supplementary material online, *Figure S12H*) as compared to NS control. In contrast, the miR-369-3p mimic treated mice exhibited increased levels of the anti-inflammatory cytokine IL-10 (see Supplementary material online, *Figure S12B*). Collectively, these results indicate suppression of GPR91-mediated inflammasome activation upon miR-369-3p mimic administration in diabetes-associated atherosclerotic mice.

We next investigated the effect of restoring miR-369-3p on the composition of circulating leukocytes. While the percentage of total monocytes (see Supplementary material online, *Figure S13B*) remained unchanged between 369-m and NS-m groups, there were significant differences in the composition of monocytes subsets between the two groups. miR-369-3p restoration increased the percentage of Ly6C^{lo} monocytes (considered to be anti-inflammatory M2-like macrophages)[65] while it reduced Ly6C^{hi} monocytes (considered to be pro-inflammatory M1-like macrophages)[66] (see Supplementary material online, *Figure S13A, C and D*). No significant changes were observed in neutrophils (see Supplementary material online, *Figure S13E*), B cells (see Supplementary material online, *Figure S13F*), CD3+ T cells (see Supplementary material online, *Figure S13G*), and CD8 + T cells (see Supplementary material online, *Figure S13H*), while a modest non-significant increase in circulating CD4+ T cells (see Supplementary material online, *Figure S13I*) was observed in the miR-369-treated group compared to the NS control group. Flow cytometric analyses showed a robust decrease in inflammatory (M1-like) plaque macrophages (CD11b + CD11c + CD206−) and an increase in pro-resolving M2-like macrophages (CD11b + CD11c − CD206 +) in mice treated with miR-369-3p mimic compared to the NS controls (*Figure 7D, E* and Supplementary material online, *Figure S14*). This was accompanied by a decrease in expression of M1 markers, CCR2 (*Figure 7F*) and CD86 (*Figure 7G*) and an increase in the expression of the M2 marker, arginase (Arg1) (*Figure 7H*). In line with these findings, the Ingenuity Pathway Analyses (IPA) of differentially expressed genes in miR-369 treated mice identified pathways related to phagosome formation (a known characteristic of pro-resolving, alternatively activated M2 macrophages) as the most enriched BP in aortic macrophages from the miR-369-3p mimic treated mice compared to NS control mice (see Supplementary material online, *Figure S11B*).

3.10 miR-369-3p restoration increases the accumulation of pro-resolving M2-like macrophages in diabetes-associated atherosclerotic lesions

Activated M2 macrophages are known to efficiently clear apoptotic cells, a process known as efferocytosis and is essential for tissue repair and homeostasis.[67,68] However, chronic inflammation states, such as in atherosclerosis, exhibit reduced levels of M2-like macrophages and consequently defective efferocytosis and formation of necrotic cores in lesions. In addition, M2 macrophages express high levels of Arginase 1 and have increased secretion of collagen, which could promote tissue repair and plaque stability.[69,70] Because our IPA analyses and flow cytometric analyses indicated a favourable pro-resolving macrophage phenotype as well as enrichment of genes associated with phagosome formation in the miR-369 treatment group, we sought to investigate the extent of necrosis and markers of macrophage efferocytosis in aortic lesions of both groups. Intriguingly, co-staining of aortic lesions for TUNEL and the macrophage marker Mac-2 showed a significant increase in macrophage-bound compared to free apoptotic cells in aortic lesions of miR-369-m compared to NS control treated mice (see Supplementary material online, *Figure S15A–C*), whereas free apoptotic (TUNEL+) cells were reduced (see Supplementary material online, *Figure S15B*). These findings indicate that administration of miR-369-3p mimics increased macrophage efferocytosis in diabetes-associated atherosclerotic lesions, thereby contributing to the reduction of atherosclerosis plaque burden. Consistent with these findings, plaque necrosis was also reduced in aortic lesions from miR-369-treated mice compared to NS injected mice (see Supplementary material online, *Figure S15D and E*). Taken together, these findings reveal a critical *in vivo* role of miR-369-3p in suppressing GPR91-mediated inflammasome activation and promoting a pro-resolving macrophage phenotype that contributes to the amelioration of diabetes-associated atherosclerosis progression.

3.11 GPR91 is up-regulated in PBMCs from patients with diabetes and CAD and is involved in regulating monocyte inflammation

Our findings reveal that GPR91 is a direct target of miR-369-3p. GPR91 is implicated in regulating inflammation,[53] however, it is unknown if GPR91 expression is altered in patients with diabetes and CAD. To extend the clinical significance of our findings, we isolated PBMCs from patients with CAD (with and without diabetes) and assessed GPR91 transcript expression. Consistent with our preclinical studies, GPR91 expression increased in patients with diabetes and CAD (*Figure 8A*). Next, to explore the effects of oxLDL on miR-369-3p and GPR91 in human monocytes, we isolated primary monocytes from PBMCs from healthy subjects. We found that oxLDL-loading in human monocytes markedly reduced miR-369-3p expression, which occurred in parallel to an increase in sucnr1/GPR91 and IL-1β expression (*Figure 8B–E*), consistent with the *in vivo* observations. Finally, to identify the therapeutic benefits of targeting GPR91, we treated primary monocytes from human subjects with or without diabetes with a human-specific GPR91 antagonist (NF-56-EJ40) in the presence of oxLDL-treatment. OxLDL-loading significantly increased the IL-1β secretion in healthy and diabetic monocytes compared to control. In contrast, blocking of GPR91 signalling significantly reduced IL-1β in the presence of the GPR91 antagonist (*Figure 8E* and *F*), suggesting a therapeutic role of blocking GPR91 signalling in regulating inflammation in human monocytes.

4. Discussion

Despite optimal glycaemic control and successful lipid lowering strategies, individuals with diabetes exhibit accelerated development of atherosclerotic plaques. Diabetes skews monocyte/macrophage metabolism and an inflammatory phenotype that promotes plaque burden. Identifying a key regulator capable of dampening metabolic inflammation is an important, yet unmet therapeutic need. We discovered a novel role of miR-369-3p in regulating metabolic inflammation in macrophages through a succinate-GPR91 inflammatory signalling pathway. Our study found reduced miR-369-3p expression in inflammatory macrophages in mice, and in PBMCs from patients with diabetes and CAD. Given the macrophage-enriched expression of miR-369-3p, the downregulation of miR-369-3p in human PBMCs is likely attributed to the large percentage of monocyte/macrophage population in PBMCs. In an idiopathic pulmonary fibrosis model, LPS-mediated lung inflammation down-regulated miR-369-3p expression.[71] In addition, a recent report highlighted the downregulation of serum levels of miR-369-3p in COVID-19 infected patients.[72] In dendritic cells, LPS-induced inflammation also down-regulated miR-369-3p expression.[44,73] Pro-inflammatory markers IL-6, IL-1β, and tumour necrosis factor (TNF)-α, and cell death were also suppressed in miR-369-3p overexpressing cardiomyocytes.[74] In another report, miR-369-3p was shown to ameliorate intestinal inflammatory responses by dampening BRCC3 expression in macrophages.[38] Consistent with this specific role for miR-369-3p in regulating inflammation, our study provides *in vitro*, *in vivo* and translational evidence that: (i) miR-369-3p ameliorates oxLDL-mediated mitochondrial stress and inflammasome activation by regulating succinate-GPR91 signalling; (ii) therapeutic delivery of miR-369-3p halts the progression of diabetes-associated atherosclerosis in mice by suppressing the plaque macrophage inflammatory signals, in part by regulating GPR91 signalling; and iii) blockade of GPR91 signalling suppressed inflammasome activation as observed by significant reduction in IL-1β release in primary monocytes from human subjects with diabetes.

Mitochondrial dysfunction and metabolic inflammation are classic features of diabetes. Of note, oxLDL-mediated inflammation disrupts

Downloaded from https://academic.oup.com/cardiovascres/advance-article/doi/10.1093/cvr/cvae102/7664626 by Ewha Womans University user on 02 September 2024

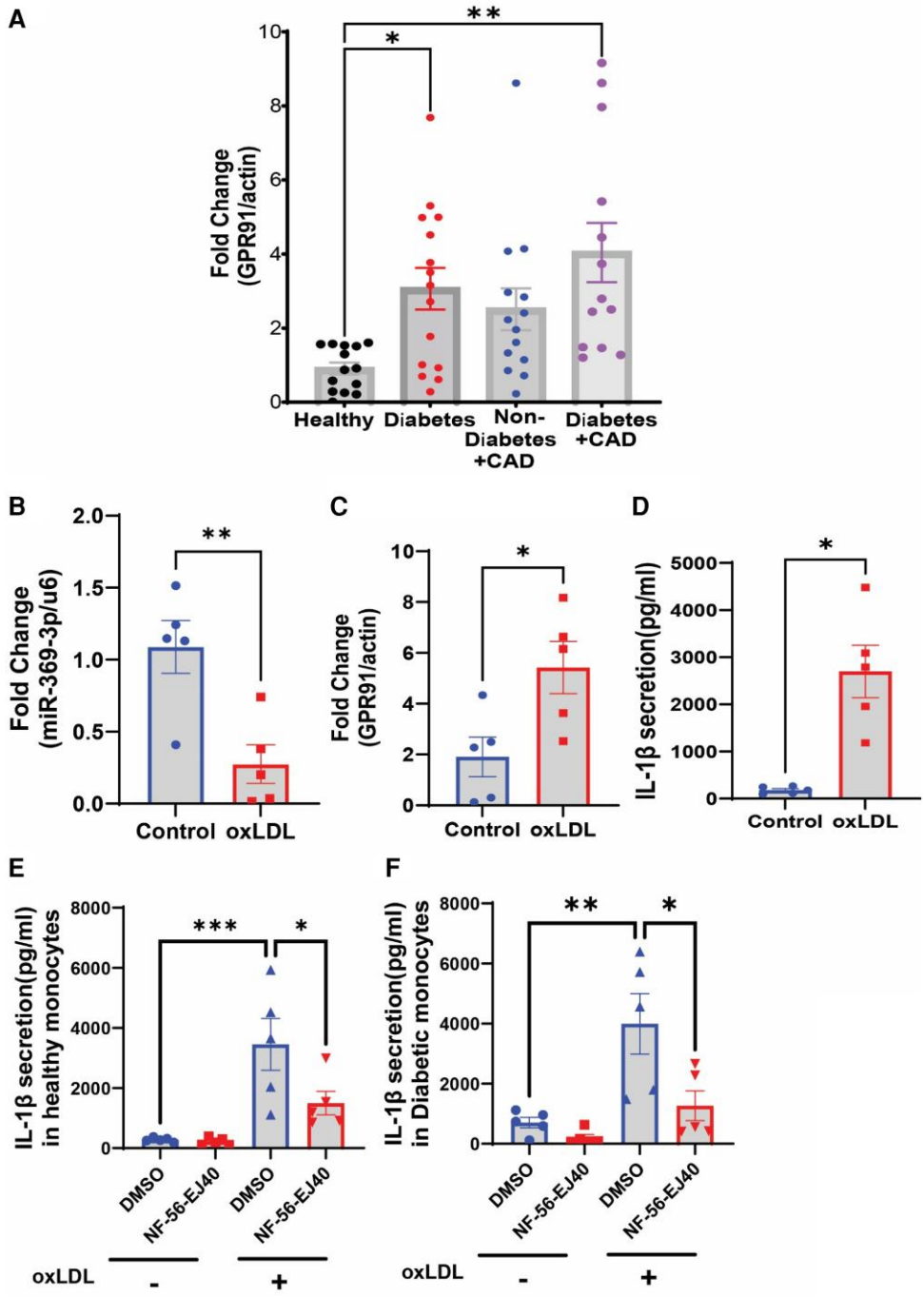

Figure 8 GPR91 is up-regulated in PBMCs from patients with diabetes and CAD and by oxLDL in primary human monocytes. (*A*) RT-qPCR analysis of SUCNR1/GPR91 expression in human PBMCs (healthy controls, DM, CAD, or DM + CAD ($n = 11$–15/group). (*B* and *C*) Primary human monocytes were serum-starved overnight and oxLDL was loaded for 24 h. RNA was isolated, and RT-qPCR was performed to determine miRNA-369-3p (*B*) and GPR91 (*C*) expression. (*D*) ELISA was performed on cell supernatants to detect IL-1β secretion. (*E* and *F*) Primary monocytes from human subjects without (*E*) or with diabetes (*F*) were either untreated or pre-treated with human-specific GPR91 inhibitor, NF-56-EJ40 for 1 h, followed by oxLDL-loading for 24 h and ELISA was performed on cell supernatants to detect IL-1β ($N = 5$ biological replicates per group). Statistical analysis was performed using unpaired Student's *t*-test (*B*–*D*) or using one-way ANOVA followed by Holm-Šídák test for multiple comparisons (*A* and *E*). All data are mean ± SEM. Statistical differences are indicated as $^{*}P < 0.05$; $^{**}P < 0.01$; $^{***}P < 0.001$; and $^{****}P < 0.0001$ vs. NS-m control.

the TCA cycle and increases the glycolysis pathway over OXPHOS for energy production.[75] Our discovery shows a novel role for miR-369-3p in positively regulating mitochondrial homeostasis by reducing glycolysis and restoring OXPHOS in oxLDL-loaded BMDMs. Importantly, the increase in markers of mitochondrial dysfunction (p-DRP1, p-ERK1/2) in BMDMs with miR-369-3p inhibition highlighted the impact of miR-369-3p deficiency on macrophage mitochondrial stress.

Downloaded from https://academic.oup.com/cardiovascres/advance-article/doi/10.1093/cvr/cvae102/7664626 by Ewha Womans University user on 02 September 2024

Disruption of the TCA cycle alters metabolite levels, especially succinate, fumarate, and malate, propagating metabolic inflammation.[11,14] A distinct role of increased accumulation and release of succinate has been highlighted in metabolic diseases such as diabetic retinopathy, diabetic kidney disease, rheumatoid arthritis, and other chronic inflammatory diseases.[14,50,55,58] Under physiological conditions, succinate is oxidized to fumarate by the enzyme SDH in the TCA cycle to generate electrons for ATP production. In addition, the electrons generated during the conversion of succinate to fumarate in the TCA cycle can enter the electron transport chain to drive OXPHOS. However, metabolic conditions, such as diabetes can cause SDH deficiency and therefore the excess accumulation of succinate.[76] Intracellular succinate has three potential fates that are not mutually exclusive; (i) it can efflux from the cell and act as an extracellular metabolic signalling mediator by ligating to its receptor GPR91, thereby, promoting inflammation and inflammasome activation[14,77]; (ii) it can re-enter mitochondria as a respiratory substrate to drive ROS production; and/or (iii) it can enter the cytosol and causes HIF-1α stabilization by inhibiting the activity of prolyl hydroxylase domain enzymes. Notably, circulating levels of succinate are known to be elevated in patients with CAD and diabetes.[51,78] Succinate acts as an extracellular signalling mediator through its receptor GPR91, promoting inflammation and inflammasome activation.[52] As such, succinate is considered as an 'alarmin' released by macrophages in the inflammatory state. However, factors governing the succinate-GPR91 axis remained poorly understood. Using bioinformatics analyses, we discovered GPR91 as a novel and direct target of miR-369-3p and validated this interaction via 3′ UTR reporter assays. Most importantly, miR-369-3p overexpression significantly reduced intracellular and extracellular succinate levels, GPR91 expression, and the inflammasome activation. To identify if the decrease in inflammation and inflammasome activation by miR-369-3p is attributed directly to GPR91, we used three approaches: (i) using miR-369-3p inhibitor in oxLDL-loaded BMDMs; (ii) overexpressing GPR91 in oxLDL-loaded RAW 264.7 macrophages; and (iii) silencing GPR91 in oxLDL-loaded BMDMs. The miR-369-3p inhibitor as well as the overexpression of GPR91 increased GPR91 expression, NLRP3 inflammasome activation, and IL-1β secretion, whereas silencing of GPR91 profoundly reduced NLRP3 inflammasome activation and IL-1β secretion, suggesting that these effects were dependent on GPR91. Further, the silencing of GPR91 had no significant impact on the extracellular succinate release, indicating that the regulation of succinate release may be independent of GPR91 expression. As miR-369-3p overexpression significantly decreased extracellular succinate levels in oxLDL-loaded BMDMs, we conclude that this effect might be an indirect effect of miR-369-3p by maintaining the overall mitochondrial homeostasis, and therefore, the levels of TCA metabolites. Future studies will be of interest to provide deeper insights into the role of miR-369-3p in regulating both intracellular and extracellular succinate.

In contrast to our data, another report indicated that succinate treatment *in vitro* promoted M2-like polarization of macrophages.[79] In this study, myeloid-specific deletion of SUCNR1 (GPR91) was shown to promote a pro-inflammatory phenotype of macrophages. These discrepancies highlight that succinate signalling via GPR91 guides divergent responses in immune cells, which are tissue and context dependent. Activation of Gi-sub-unit may favour the pro-inflammatory phenotype while activation of the Gq subunit can promote an anti-inflammatory phenotype as previously discussed.[53] Nevertheless, our findings are consistent with reports from diabetic patients and mice,[51,80] indicating a pro-inflammatory role for succinate-GPR91 signalling in macrophage inflammation. In support of the pro-inflammatory effects of succinate, we observed that priming of mouse primary monocytes with succinate prior to oxLDL-treatment exacerbated the pro-inflammatory phenotype of monocytes. This suggests that succinate can induce a pro-inflammatory phenotype under atherogenic stimuli. Succinate accumulation is known to stabilize HIF-1α expression and promote inflammatory gene expression.[14] We observed a similar phenomenon where oxLDL-mediated accumulation of succinate increased HIF-1α expression, while miR-369-3p overexpression reduced HIF-1α expression. Since HIF-1α is not a direct target of miR-369-3p, we hypothesize that the repression of HIF-1α is an indirect effect of miR-369-3p via regulating overall cellular energetics and likely by modulating succinate levels.

Consistent with previous reports, results from our study demonstrate that oxLDL increases mitochondrial damage, associated with altered cellular metabolites, likely due to increased ROS production. Because miR-369-3p served an important role in mediating mitochondrial stress via repressing GPR91 and p-DRP1, we speculated if the increased ROS production by oxLDL leads to increased GPR91 expression in macrophage foam cells. Consistent with this hypothesis, ROS inhibition using NAC in oxLDL-treated foam cells reduced the GPR91 expression and its downstream inflammasome activation marker NLRP3.

Because miR-369-3p was markedly reduced in response to pro-inflammatory stimuli in macrophages in vitro, and from intimal lesions of atherosclerotic mice, in vivo, we raised the possibility of miR-369-3p 'replacement therapy', as our findings demonstrated a protective role in normalizing metabolic inflammation *in vitro*. Indeed, miR-369-3p overexpression in *Ldlr*−/− HFSC mice halted atherosclerotic progression and decreased serum pro-inflammatory cytokines. Moreover, therapeutic administration of miR-369-3p mimic not only reduced GPR91, NLRP3, and inflammatory macrophage markers in the plaque, but also enhanced the functionality of macrophages, specifically by enriching M2-like pro-resolving macrophages in lesions of diabetic atherogenic mice. Additionally, restoration of miR-369-3p in aortic macrophages increased their ability to clear apoptotic cells and impart plaque stability as evident by increased efferocytosis and reduced plaque necrosis. As such, miR-369-3p is a pleiotropic regulator of metabolic and inflammatory processes in atherosclerotic plaques and consequently promotes diabetic atherosclerosis regression. These findings are notable in that there were no changes in the glucose or insulin tolerance in mice administered miR-369-3p mimic, which suggested a specific and prominent role of miR-369-3p in regulating metabolic inflammation.

A few limitations of the study include the recognition that though miR-369-3p is enriched in macrophages, it is also expressed in other immune cells and non-immune cells as we have shown in our cell-type profiling. This study was focused on the role of miR-369-3p in macrophages; however, we hypothesize that the anti-inflammatory or pro-resolving effect of miR-369-3p overexpression *in vivo* may also be conferred by other regulatory immune cells, which may further indirectly influence macrophage function and metabolism. The precise mechanisms governing the ability of miR-369-3p in regulating oxLDL-induced intracellular and extracellular succinate levels and the relative contribution of GPR91 *in vivo* is an intriguing avenue for further investigation. Future studies will be needed to elucidate the direct or indirect interactions between miR-369-3p expression and activity of enzymes involved in succinate metabolism in response to miR-369-3p modulation. The contribution of immunometabolites other than succinate is also not a focus of this study, but future investigation will be required to address this possibility. GPR91 is well-studied in macrophages; however, it is also expressed in other cell-types. Given miR-369-3p expression in cell-types other than macrophages, it will be of interest to explore the potential contributing role of miR-369-3p-mediated regulation of the succinate-GPR91 axis elsewhere in future studies. In addition, future studies using GPR91 knockout mice will further help to strengthen our current findings on the impact of miR-369-3p regulation on GPR91 signalling in diabetes-associated atherosclerosis. We also acknowledge the fact that there could be potential downstream targets of miR-369-3p beyond GPR91 that are attributable towards the therapeutic benefits of miR-369-3p *in vivo*. Lastly, the current study only used male Ldlr−/− mice based on prior findings of aggravated atherogenesis in male Ldlr−/− mice on a high-fat sucrose-containing diet.[81] However, future studies will be of interest to understand if there may be sex-specific roles for miR-369-3p and the succinate-GPR91 signalling pathway.

In summary, this study highlights a multifaceted role of miR-369-3p in regulating inflammation, mitochondrial stress, and inflammasome activation in lipid-laden foam cells, at least in part, by targeting the metabolite succinate and its cognate receptor GPR91 in diabetes-associated atherosclerosis. Expression of the monocyte/macrophage-enriched miR-369-3p is markedly reduced in macrophages and in PBMCs-derived from human subjects with diabetes and diabetes-associated CAD and was coupled with the increase of SUCR1/GPR91 expression in those samples. Therapeutic delivery of miR-369-3p in an advanced diabetic atherosclerosis *in vivo* model showed marked reduction in plaque progression and

Downloaded from https://academic.oup.com/cardiovascres/advance-article/doi/10.1093/cvr/cvae102/7664626 by Ewha Womans University user on 02 September 2024

reduced inflammation in plaque macrophages. The data presented in this study highlights a promising therapeutic potential of miR-369-3p to reduce or resolve metabolic inflammation in a range of diabetes-associated vascular disease states.

Translational perspective

Patients with diabetes are at a higher risk of complications from accelerated atherosclerosis such as heart attack, stroke, and peripheral artery disease. Diabetes is known to promote both systemic and atherosclerotic plaque inflammation, leading to dysregulated macrophage metabolism and a skewing towards a pro-inflammatory macrophage phenotype. However, the role of microRNAs in this process are still poorly understood. This study identified a novel role for the macrophage-enriched miR-369-3p in regulating macrophage immunometabolism in diabetes-accelerated atherosclerosis by suppressing a succinate-GPR91-inflammasome signalling pathway. Restoration of miR-369-3p may serve as a promising approach to diabetes-associated atherosclerosis.

Supplementary material

Supplementary material is available at *Cardiovascular Research* online.

Acknowledgement

The authors wish to acknowledge John M. Asara from the Mass Spectrometry Core Facility, Beth Israel Deaconess Medical Center for technical expertise for the mass spectrometry analyses. We thank Lay-Hong Ang for use of the confocal imaging core (Harvard Digestive Disease Center, NIH P30DK034854).

Conflict of interest: none declared.

Funding

This work was supported by the National Institutes of Health (HL115141, HL134849, HL148207, HL148355, HL153356, and HL167905 to M.W.F.), and the American Heart Association (18SFRN33900144 and 20SFRN35 200163 to M.W.F.).

Data availability

The data underlying this article are available in the article and in its online supplementary material as well as in data repository GEO accession No. GSE244760.

References

1. Haffner SM. Diabetes, hyperlipidemia, and coronary artery disease. *Am J Cardiol* 1999;**83**:17F–21F.
2. Haffner SM. Epidemiology of insulin resistance and its relation to coronary artery disease. *Am J Cardiol* 1999;**84**:11J–14J.
3. Armitage J, Bowman L. Cardiovascular outcomes among participants with diabetes in the recent large statin trials. *Curr Opin Lipidol* 2004;**15**:439–446.
4. Evans JL, Goldfine ID, Maddux BA, Grodsky GM. Oxidative stress and stress-activated signaling pathways: a unifying hypothesis of type 2 diabetes. *Endocr Rev* 2002;**23**:599–622.
5. Lamharzi N, Renard CB, Kramer F, Pennathur S, Heinecke JW, Chait A, Bornfeldt KE. Hyperlipidemia in concert with hyperglycemia stimulates the proliferation of macrophages in atherosclerotic lesions: potential role of glucose-oxidized LDL. *Diabetes* 2004;**53**:3217–3225.
6. Russo S, Kwiatkowski M, Govorukhina N, Bischoff R, Melgert BN. Meta-inflammation and metabolic reprogramming of macrophages in diabetes and obesity: the importance of metabolites. *Front Immunol* 2021;**12**:746151.
7. Bouchareychas L, Duong P, Phu TA, Alsop E, Meechoovet B, Reiman R, Ng M, Yamamoto R, Nakauchi H, Gasper WJ. High glucose macrophage exosomes enhance atherosclerosis by driving cellular proliferation & hematopoiesis. *iScience* 2021;**24**:102847.
8. Williams NC, O'Neill LAJ. A role for the Krebs cycle intermediate citrate in metabolic reprogramming in innate immunity and inflammation. *Front Immunol* 2018;**9**:141.
9. Sun L, Zhang H, Gao P. Metabolic reprogramming and epigenetic modifications on the path to cancer. *Protein Cell* 2022;**13**:877–919.
10. Pirola L, Balcerczyk A, Tothill RW, Haviv I, Kaspi A, Lunke S, Ziemann M, Karagiannis T, Tonna S, Kowalczyk A, Beresford-Smith B, Macintyre G, Kelong M, Hongyu Z, Zhu J, El-Osta A. Genome-wide analysis distinguishes hyperglycemia regulated epigenetic signatures of primary vascular cells. *Genome Res* 2011;**21**:1601–1615.
11. Murphy MP, O'Neill LAJ. Krebs cycle reimagined: the emerging roles of succinate and itaconate as signal transducers. *Cell* 2018;**174**:780–784.
12. Martínez-Reyes I, Chandel NS. Mitochondrial TCA cycle metabolites control physiology and disease. *Nat Commun* 2020;**11**:102.
13. Jha AK, Huang SC-C, Sergushichev A, Lampropoulou V, Ivanova Y, Loginicheva E, Chmielewski K, Stewart KM, Ashall J, Everts B, Pearce EJ, Driggers EM, Artyomov MN. Network integration of parallel metabolic and transcriptional data reveals metabolic modules that regulate macrophage polarization. *Immunity* 2015;**42**:419–430.
14. Tannahill GM, Curtis AM, Adamik J, Palsson-McDermott EM, McGettrick AF, Goel G, Frezza C, Bernard NJ, Kelly B, Foley NH, Zheng L, Gardet A, Tong Z, Jany SS, Corr SC, Haneklaus M, Caffrey BE, Pierce K, Walmsley S, Beasley FC, Cummins E, Nizet V, Whyte M, Taylor CT, Lin H, Masters SL, Gottlieb E, Kelly VP, Clish C, Auron PE, Xavier RJ, O'Neill LAJ. Succinate is an inflammatory signal that induces IL-1β through HIF-1α. *Nature* 2013;**496**:238–242.
15. Rawal S, Manning P, Katare R. Cardiovascular microRNAs: as modulators and diagnostic biomarkers of diabetic heart disease. *Cardiovasc Diabetol* 2014;**13**:44.
16. Haemmig S, Yang D, Sun X, Das D, Ghaffari S, Molinaro R, Chen L, Deng Y, Freeman D, Moullan N, Tesmenitsky Y, Wara A, Simion V, Shvartz E, Lee JF, Yang T, Sukova G, Marto JA, Stone PH, Lee WL, Auwerx J, Libby P, Feinberg MW. Long noncoding RNA SNHG12 integrates a DNA-PK-mediated DNA damage response and vascular senescence. *Sci Transl Med* 2020;**12**:eaaw1868.
17. Horie T, Baba O, Kuwabara Y, Chujo Y, Watanabe S, Kinoshita M, Horiguchi M, Nakamura T, Chonabayashi K, Hishizawa M, Hasegawa K, Kume N, Yokode M, Kita T, Kimura T, Ono K. MicroRNA-33 deficiency reduces the progression of atherosclerotic plaque in ApoE-/- mice. *J Am Heart Assoc* 2012;**1**:e003376.
18. Canfrán-Duque A, Rotllan N, Zhang X, Fernández-Fuertes M, Ramírez-Hidalgo C, Araldi E, Daimiel L, Busto R, Fernández-Hernando C, Suárez Y. Macrophage deficiency of miR-21 promotes apoptosis, plaque necrosis, and vascular inflammation during atherogenesis. *EMBO Mol Med* 2017;**9**:1244–1262.
19. Afonso MS, Sharma M, Schlegel M, Solingen CV, Koelwyn GJ, Shanley LC, Beckett L, Peled D, Rahman K, Giannarelli C, Li H, Brown EJ, Khodadadi-Jamayran A, Fisher EA, Moore KJ. miR-33 silencing reprograms the immune cell landscape in atherosclerotic plaques. *Cir. Res* 2021;**128**:1122–1138.
20. Rawal S, Munasinghe PE, Shindikar A, Paulin J, Cameron V, Manning P, Williams MJ, Jones GT, Bunton R, Galvin I, Katare R. Down-regulation of proangiogenic microRNA-126 and microRNA-132 are early modulators of diabetic cardiac microangiopathy. *Cardiovasc Res* 2017;**113**:90–101.
21. Rawal S, Nagesh PT, Coffey S, Van Hout I, Galvin IF, Bunton RW, Davis P, Williams MJA, Katare R. Early dysregulation of cardiac-specific microRNA-208a is linked to maladaptive cardiac remodelling in diabetic myocardium. *Cardiovasc Diabetol* 2019;**18**:13.
22. Niu M, Li H, Li X, Yan X, Ma A, Pan X, Zhu X. Circulating exosomal miRNAs as novel biomarkers perform superior diagnostic efficiency compared with plasma miRNAs for large-artery atherosclerosis stroke. *Front Pharmacol* 2021;**12**:791644.
23. Wysoczynski M, Kim J, Moore JB 4th, Uchida S. Macrophage long non-coding RNAs in pathogenesis of cardiovascular disease. *Noncoding RNA* 2020;**6**:28.
24. Yao Q, Song Z, Wang B, Zhang JA. Emerging roles of microRNAs in the metabolic control of immune cells. *Cancer Lett* 2018;**433**:10–17.
25. Herrera BM, Lockstone HE, Taylor JM, Ria M, Barrett A, Collins S, Kaisaki P, Argoud K, Fernandez C, Travers ME, Grew JP, Randall JC, Gloyn AL, Gauguier D, McCarthy MI, Lindgren CM. Global microRNA expression profiles in insulin target tissues in a spontaneous rat model of type 2 diabetes. *Diabetologia* 2010;**53**:1099–1109.
26. Alam MM, O'neill LA. MicroRNAs and the resolution phase of inflammation in macrophages. *Eur J Immunol* 2011;**41**:2482–2485.
27. Avci CB, Baran Y. Use of microRNAs in personalized medicine. *Methods Mol Biol*. 2014;**1107**:311–325.
28. Simion V, Zhou H, Haemmig S, Pierce JB, Mendes S, Tesmenitsky Y, Pérez-Cremades D, Lee JF, Chen AF, Ronda N, Papotti B, Marto JA, Feinberg MW. A macrophage-specific lncRNA regulates apoptosis and atherosclerosis by tethering HuR in the nucleus. *Nat Commun* 2020;**11**:6135.
29. Novák J, Olejníčková V, Tkáčová N, Santulli G. Mechanistic role of microRNAs in coupling lipid metabolism and atherosclerosis. *Adv Exp Med Biol* 2015;**887**:79–100.

Downloaded from https://academic.oup.com/cardiovascres/advance-article/doi/10.1093/cvr/cvae102/7664626 by Ewha Womans University user on 02 September 2024

30. Wara AK, Rawal S, Yang X, Pérez-Cremades D, Sachan M, Chen J, Feinberg MW. KLF10 deficiency in CD4+ T cells promotes atherosclerosis progression by altering macrophage dynamics. *Atherosclerosis* 2022;**359**:27–41.
31. Ying W, Gao H, Dos Reis FCG, Bandyopadhyay G, Ofrecio JM, Luo Z, Ji Y, Jin Z, Ly C, Olefsky JM. MiR-690, an exosomal-derived miRNA from M2-polarized macrophages, improves insulin sensitivity in obese mice. *Cell Metab* 2021;**33**:781–790.e5.
32. Wara AK, Wang S, Wu C, Fang F, Haemmig S, Weber BN, Aydogan CO, Tesmenitsky Y, Aliakbarian H, Hawse JR, Subramaniam M, Zhao L, Sage PT, Tavakkoli A, Garza A, Lynch L, Banks AS, Feinberg MW. KLF10 deficiency in CD4+ T cells triggers obesity, insulin resistance, and fatty liver. *Cell Rep* 2020;**33**:108550.
33. Strauss L, Mahmoud MAA, Weaver JD, Tijaro-Ovalle NM, Christofides A, Wang Q, Pal R, Yuan M, Asara J, Patsoukis N, Boussiotis VA. Targeted deletion of PD-1 in myeloid cells induces antitumor immunity. *Sci Immunol* 2020;**5**:eaay1863.
34. Dallons M, Alpan E, Schepkens C, Tagliatti V, Colet JM. GPR91 receptor mediates protection against doxorubicin-induced cardiotoxicity without altering its anticancer efficacy. An in vitro study on H9C2 cardiomyoblasts and breast cancer-derived MCF-7 cells. *Cells* 2020;**9**:2177.
35. Hartman ML, Shirihai OS, Holbrook M, Xu G, Kocherla M, Shah A, Fetterman JL, Kluge MA, Frame AA, Hamburg NM, Vita JA. Relation of mitochondrial oxygen consumption in peripheral blood mononuclear cells to vascular function in type 2 diabetes mellitus. *Vasc Med* 2014;**19**:67–74.
36. Chen J, Zhuang R, Cheng HS, Jamaiyar A, Assa C, McCoy M, Rawal S, Pérez-Cremades D, Feinberg MW. Isolation and culture of murine aortic cells and RNA isolation of aortic intima and media: rapid and optimized approaches for atherosclerosis research. *Atherosclerosis* 2022;**347**:39–46.
37. Zhang E, Wu Y. MicroRNAs: important modulators of oxLDL-mediated signaling in atherosclerosis. *J Atheroscler Thromb* 2013;**20**:215–227.
38. Scalavino V, Piccinno E, Valentini AM, Schena N, Armentano R, Giannelli G, Serino G. miR-369-3p modulates intestinal inflammatory response via BRCC3/NLRP3 inflammasome axis. *Cells* 2023;**12**:2184.
39. O'Neill LA, Kishton RJ, Rathmell J. A guide to immunometabolism for immunologists. *Nat Rev Immunol* 2016;**16**:553–565.
40. Suárez-Rivero JM, Pastor-Maldonado CJ, Povea-Cabello S, Álvarez-Córdoba M, Villalón-García I, Talaverón-Rey M, Suárez-Carrillo A, Munuera-Cabeza M, Sánchez-Alcázar JA. From mitochondria to atherosclerosis: *the inflammation path*. *Biomedicines* 2021;**9**:258.
41. Zmijewski JW, Moellering DR, Le Goffe C, Landar A, Ramachandran A, Darley-Usmar VM. Oxidized LDL induces mitochondrially associated reactive oxygen/nitrogen species formation in endothelial cells. *Am J Physiol Heart Circ Physiol* 2005;**289**:H852–H861.
42. Shatrov VA, Sumbayev VV, Zhou J, Brüne B. Oxidized low-density lipoprotein (oxLDL) triggers hypoxia-inducible factor-1alpha (HIF-1alpha) accumulation via redox-dependent mechanisms. *Blood* 2003;**101**:4847–4849.
43. Liu W, Yin Y, Zhou Z, He M, Dai Y. OxLDL-induced IL-1 beta secretion promoting foam cells formation was mainly via CD36 mediated ROS production leading to NLRP3 inflammasome activation. *Inflamm Res* 2014;**63**:33–43.
44. Scalavino V, Liso M, Cavalcanti E, Gigante I, Lippolis A, Mastronardi M, Chieppa M, Serino G. miR-369-3p modulates inducible nitric oxide synthase and is involved in regulation of chronic inflammatory response. *Sci Rep* 2020;**10**:15942.
45. Sohrabi Y, Lagache SMM, Schnack L, Godfrey R, Kahles F, Bruemmer D, Waltenberger J, Findeisen HM. mTOR-dependent oxidative stress regulates oxLDL-induced trained innate immunity in human monocytes. *Front Immunol* 2019;**9**:3155.
46. Chen Y, Yang M, Huang W, Chen W, Zhao Y, Schulte ML, Volberding P, Gerbec Z, Zimmermann MT, Zeighami A, Demos W, Zhang J, Knaack DA, Smith BC, Cui W, Malarkannan S, Sodhi K, Shapiro JI, Xie Z, Sahoo D, Silverstein RL. Mitochondrial metabolic reprogramming by CD36 signaling drives macrophage inflammatory responses. *Circ Res* 2019;**125**:1087–1102.
47. Mills E, O'Neill LAJ. Succinate: a metabolic signal in inflammation. *Trends Cell Biol* 2014;**24**:313–320.
48. Smestad J, Erber L, Chen Y, Maher LJ3rd. Chromatin succinylation correlates with active gene expression and is perturbed by defective TCA cycle metabolism. *iScience* 2018;**2**:63–75.
49. Kula-Alwar D, Prag HA, Krieg T. Targeting succinate metabolism in ischemia/reperfusion injury. *Circulation* 2019;**140**:1968–1970.
50. Hu J, Li T, Du X, Wu Q, Le Y-Z. G protein-coupled receptor 91 signaling in diabetic retinopathy and hypoxic retinal diseases. *Vision Res* 2017;**139**:59–64.
51. van Diepen JA, Robben JH, Hooiveld GJ, Carmone C, Alsady M, Boutens L, Bekkenkamp-Grovenstein M, Hijmans A, Engelke UFH, Wevers RA, Netea MG, Tack CJ, Stienstra R, Deen PMT. SUCNR1-mediated chemotaxis of macrophages aggravates obesity-induced inflammation and diabetes. *Diabetologia* 2017;**60**:1304–1313.
52. Mills EL, Kelly B, Logan A, Costa ASH, Varma M, Bryant CE, Tourlomousis P, Däbritz JHM, Gottlieb E, Latorre I, Corr SC, McManus G, Ryan D, Jacobs HT, Szibor M, Xavier RJ, Braun T, Frezza C, Murphy MP, O'Neill LA. Succinate dehydrogenase supports metabolic repurposing of mitochondria to drive inflammatory macrophages. *Cell* 2016;**167**:457–470.e13.
53. Krzak G, Willis CM, Smith JA, Pluchino S, Peruzzotti-Jametti L. Succinate receptor 1: an emerging regulator of myeloid cell function in inflammation. *Trends Immunol* 2021;**42**:45–58.
54. Li T, Hu J, Du S, Chen Y, Wang S, Wu Q. ERK1/2/COX-2/PGE2 signaling pathway mediates GPR91-dependent VEGF release in streptozotocin-induced diabetes. *Mol Vis* 2014;**20**:1109–1121.
55. Littlewood-Evans A, Sarret S, Apfel V, Loesle P, Dawson J, Zhang J, Muller A, Tigani B, Kneuer R, Patel S, Valeaux S, Gommermann N, Rubic-Schneider T, Junt T, Carballido JM. GPR91 senses extracellular succinate released from inflammatory macrophages and exacerbates rheumatoid arthritis. *J Exp Med* 2016;**213**:1655–1662.
56. Fremder M, Kim SW, Khamaysi A, Shimshilashvili L, Eini-Rider H, Park IS, Hadad U, Cheon JH, Ohana E. A transepithelial pathway delivers succinate to macrophages, thus perpetuating their pro inflammatory metabolic state. *Cell Rep* 2021;**36**:109521.
57. Li L, Dong Y-L, Liu T, Luo D, Wei C, Shi W-Y. Increased succinate receptor GPR91 involved in the pathogenesis of Mooren's ulcer. *Int J Ophthalmol* 2018;**11**:1733–1740.
58. Toma I, Kang JJ, Sipos A, Vargas S, Bansal E, Hanner F, Meer E, Peti-Peterdi J. Succinate receptor GPR91 provides a direct link between high glucose levels and renin release in murine and rabbit kidney. *J Clin Invest* 2008;**118**:2526–2534.
59. Lu Y-T, Li L-Z, Yang Y-L, Yin X, Liu Q, Zhang L, Liu K, Liu B, Li J, Qi L-W. Succinate induces aberrant mitochondrial fission in cardiomyocytes through GPR91 signaling. *Cell Death Dis* 2018;**9**:672.
60. Zhou K, Shi L, Wang Z, Zhou J, Manaenko A, Reis C, Chen S, Zhang J. RIP1-RIP3-DRP1 pathway regulates NLRP3 inflammasome activation following subarachnoid hemorrhage. *Exp Neurol* 2017;**295**:116–124.
61. Xin T, Lu C, Zhang J, Wen J, Yan S, Li C, Zhang F, Zhang J. Oxidized LDL disrupts metabolism and inhibits macrophage survival by activating a miR-9/Drp1/mitochondrial fission signaling pathway. *Oxid Med Cell Longev* 2020;**2020**:8848930.
62. Kashatus JA, Nascimento A, Myers LJ, Sher A, Byrne FL, Hoehn KL, Counter CM, Kashatus DF. Erk2 phosphorylation of Drp1 promotes mitochondrial fission and MAPK-driven tumor growth. *Mol Cell* 2015;**57**:537–551.
63. Bae YS, Lee JH, Choi SH, Kim S, Almazan F, Witztum JL, Miller YI. Macrophages generate reactive oxygen species in response to minimally oxidized low-density lipoprotein: toll-like receptor 4- and spleen tyrosine kinase-dependent activation of NADPH oxidase 2. *Circ Res* 2009;**104**:210–218. 21p following 218.
64. Jiang Q, Chen Q, Li C, Gong Z, Li Z, Ding S. Ox-LDL-induced endothelial progenitor cell oxidative stress via p38/Keap1/Nrf2 pathway. *Stem Cells Int* 2022;**2022**:5897194.
65. Brunet A, LeBel M, Egarnes B, Paquet-Bouchard C, Lessard AJ, Brown JP, Gosselin J. NR4A1-dependent Ly6C^{low} monocytes contribute to reducing joint inflammation in arthritic mice through Treg cells. *Eur J Immunol* 2016;**46**:2789–2800.
66. Menke J, Rabacal WA, Byrne KT, Iwata Y, Schwartz MM, Stanley ER, Schwarting A, Kelley VR. Circulating CSF-1 promotes monocyte and macrophage phenotypes that enhance lupus nephritis. *J Am Soc Nephrol* 2009;**20**:2581–2592.
67. Osuna-Prieto FJ, Martinez-Tellez B, Ortiz-Alvarez L, Di X, Jurado-Fasoli L, Xu H, Ceperuelo-Mallafré V, Núñez-Roa C, Kohler I, Segura-Carretero A, García-Lario JV, Gil A, Aguilera CM, Llamas-Elvira JM, Rensen PCN, Vendrell J, Ruiz JR, Fernández-Veledo S. Elevated plasma succinate levels are linked to higher cardiovascular disease risk factors in young adults. *Cardiovasc Diabetol* 2021;**20**:151.
68. Gundra UM, Girgis NM, Ruckerl D, Jenkins S, Ward LN, Kurtz ZD, Wiens KE, Tang MS, Basu-Roy U, Mansukhani A, Allen JE, Loke P. Alternatively activated macrophages derived from monocytes and tissue macrophages are phenotypically and functionally distinct. *Blood* 2014;**123**:e110–e122.
69. Wang L, Li H, Tang Y, Yao P. Potential mechanisms and effects of efferocytosis in atherosclerosis. *Front Endocrinol (Lausanne)* 2021;**11**:585285.
70. Wang Y, Shi R, Zhai R, Yang S, Peng T, Zheng F, Shen Y, Li M, Li L. Matrix stiffness regulates macrophage polarization in atherosclerosis. *Pharmacol Res* 2022;**179**:106236.
71. Yi H, Luo D, Xiao Y, Jiang D. Knockdown of long non–coding RNA DLEU2 suppresses idiopathic pulmonary fibrosis by regulating the microRNA–369–3p/TRIM2 axis. *Int J Mol Med* 2021;**47**:80.
72. Garcia-Giralt N, Du J, Marin-Corral J, Bódalo-Torruella M, Blasco-Hernando F, Muñoz-Bermúdez R, Clarós M, Nonell L, Perera-Bel J, Fernandez-González M, Nogues X, Sorli-Redó L, Güerri-Fernández R. Circulating microRNA profiling is altered in the acute respiratory distress syndrome related to SARS-CoV-2 infection. *Sci Rep* 2022;**12**:6929.
73. Galleggiante V, De Santis S, Liso M, Verna G, Sommella E, Mastronardi M, Campiglia P, Chieppa M, Serino G. Quercetin-Induced miR-369-3p suppresses chronic inflammatory response targeting C/EBP-β. *Mol Nutr Food Res* 2019;**63**:e1801390.
74. Wang J, Chen X, Huang W. MicroRNA-369 attenuates hypoxia-induced cardiomyocyte apoptosis and inflammation via targeting TRPV3. *Braz J Med Biol Res* 2021;**54**:e10550.
75. Groh LA, Ferreira AV, Helder L, van der Heijden CDCC, Novakovic B, van de Westerlo E, Matzaraki V, Moorlag SJCFM, de Bree LC, Koeken VACM, Mourits VP, Keating ST, van Puffelen JH, Hoischen A, Joosten LAB, Netea MG, Koopman WJH, Riksen NP. oxLDL-induced trained immunity is dependent on mitochondrial metabolic reprogramming. *Immunometabolism* 2021;**3**:e210025.
76. Lee S, Xu H, Van Vleck A, Mawla AM, Li AM, Ye J, Huising MO, Annes JP. β-Cell succinate dehydrogenase deficiency triggers metabolic dysfunction and insulinopenic diabetes. *Diabetes* 2022;**71**:1439–1453.
77. Prag HA, Gruszczyk AV, Huang MM, Beach TE, Young T, Tronci L, Nikitopoulou E, Mulvey JF, Ascione R, Hadjihambi A, Shattock MJ, Pellerin L, Saeb-Parsy K, Frezza C, James AM, Krieg

Downloaded from https://academic.oup.com/cardiovascres/advance-article/doi/10.1093/cvr/cvae102/7664626 by Ewha Womans University user on 02 September 2024

T, Murphy MP, Aksentijević D. Mechanism of succinate efflux upon reperfusion of the ischaemic heart. *Cardiovasc Res* 2021;**117**:1188–1201.
78. Xu J, Zheng Y, Zhao Y, Zhang Y, Li H, Zhang A, Wang X, Wang W, Hou Y, Wang J. Succinate/IL-1β signaling axis promotes the inflammatory progression of endothelial and exacerbates atherosclerosis. *Front Immunol* 2022;**13**:817572.
79. Keiran N, Ceperuelo-Mallafré V, Calvo E, Hernández-Alvarez MI, Ejarque M, Núñez-Roa C, Horrillo D, Maymó-Masip E, Rodríguez MM, Fradera R, de la Rosa JV, Jorba R, Megia A, Zorzano A, Medina-Gómez G, Serena C, Castrillo A, Vendrell J, Fernández-Veledo S. SUCNR1 controls an anti-inflammatory program in macrophages to regulate the metabolic response to obesity. *Nat Immunol* 2019;**20**:581–592.
80. Fernández-Veledo S, Marsal-Beltran A, Vendrell J. Type 2 diabetes and succinate: unmasking an age-old molecule. *Diabetologia* 2024;**67**:430–442.
81. Chen J, Jamaiyar A, Wu W, Hu Y, Zhuang R, Sausen G, Cheng HS, de Oliveira Vaz C, Pérez-Cremades D, Tzani A, McCoy MG, Assa C, Eley S, Randhawa V, Lee K, Plutzky J, Hamburg NM, Sabatine MS, Feinberg MW. Deficiency of lncRNA MERRICAL abrogates macrophage chemotaxis and diabetes-associated atherosclerosis. *Cell Rep* 2024;**43**:113815.

Downloaded from https://academic.oup.com/cardiovascres/advance-article/doi/10.1093/cvr/cvae102/7664626 by Ewha Womans University user on 02 September 2024